# Theoretical Comparison Between Radiometric and Radiation Pressure Measurements for Determination of the Earth's Radiation Budget

by
T.H. Vonder Haar and E.A. Smith

Department of Atmospheric Science
Colorado State University
Fort Collins, Colorado

Colorado State University

Department of Atmospheric Science

Paper No. 315

# THEORETICAL COMPARISON BETWEEN RADIOMETRIC AND RADIATION PRESSURE MEASUREMENTS FOR DETERMINATION OF THE EARTH'S RADIATION BUDGET

for the

European Space Agency Headquarters

Paris, France

by

T. H. Vonder Haar and E. A. Smith

Department of Atmospheric Science

Colorado State University

Fort Collins, Colorado U.S.A.

July, 1979

Atmospheric Science Paper No. 315

TABLE OF CONTENTS

## LIST OF TABLES

## LIST OF FIGURES

# 1. SUMMARY

An analysis of the measurement of Earth Radiation Budget components by both standard radiometric principles and radiation pressure principles has been carried out in the context of a complete radiation budget experiment.

Section 2 outlines the nature and the required measurement accuracy of an Earth Radiation Budget Experiment. Section 3 is provided as a brief description of the remaining individual section topics. Section 4 covers the physical basis for both radiometric and radiation pressure measurements including discussions of the sources of error in the measurements.

A summarization of the advantages and disadvantages of the current detector technology is contained in Section 5. Section 6 outlines the actual spacecraft requirements for a global experiment. Problems associated with the processing and analysis of raw radiative measurements are given in Section 7 where it is shown that most of these problems are independent of the detection technique itself.

Section 8 contains a brief discussion of the potential benefits of a composite radiometer-radiation pressure satellite. Section 9 concludes the report with a compilation of the major findings as determined from our own research and from discussions with personnel from various ESA laboratories and other scientists. In addition to the main findings presented in the last section, a synopsis is provided at the end of all other sections.

## 2. STATEMENT OF EARTH RADIATION BUDGET SCIENTIFIC OBJECTIVES

During the last several years, in connection with the new international climate program activities, there has been special attention to new measurements of the Earth's radiation budget (COSPAR WG6, 1978). As a baseline for development of new measurement systems the U. S. space program prepared the following statement of the problem (Vonder Haar and Wallschlaeger, 1978). Note that, in general, the requirements enumerated by groups concerned with SEOCS (Sun-Earth Observatory and Climatology Satellite) and BIRAMIS (Bilan Radiatif Au Moyen D'un Microaccélérométre) parallel the requirements noted below.

Of the solar energy incident upon Earth, a portion is reflected to space while the remainder is absorbed by the Earth and its atmosphere. The absorbed energy provides the bulk of the thermal energy to the Earth and its atmospheric system and ultimately returns to space as emitted or infrared radiation. To maintain the thermal equilibrium of the Earth, the incident, reflected and emitted components of the Earth's radiation budget must be in balance. Meteorologists and climatologists agree that the spatial distributions of the Earth radiant energy budget and the temporal variations in these distributions are the fundamental physical drivers of climate. The mission for the Earth radiation budget instruments then is the measurement of the radiation budget components, i.e., the incoming solar radiation, the terrestrially reflected shortwave radiation, and the terrestrially emitted longwave radiation. Measurements made by these instruments will provide monthly averages of the radiation

components on various spatial and temporal scales. Areas of localized warming (positive net radiation) or cooling (negative net radiation) represent the energy sources and sinks that drive the atmospheric and oceanic circulations. These measurements are expected to provide improved understanding of climate and possible projections of climate trends leading to improved management, planning, and utilization of food supplies and natural resources.

The mission requirements for Earth Radiation Budget can be categorized as (a) scientific inputs concerning accuracy, reproducibility, and periodicity; (b) instrument requirements; (c) spacecraft interface constraints.

Current studies have focused on the determination of Earth radiation budget parameters at the top of the atmosphere on monthly and larger time scales for the following area resolutions:

1. 250 by 250 Km regions
2. 1000 by 1000 Km regions in the Tropics
3. $10^{o}$ Latitudinal Zones
4. Equator to Pole Gradient
5. Gobal

Values for Earth albedo or shortwave radiation, longwave radiation and net radiation (i.e., incoming solar radiation minus shortwave and longwave radiation) should be determined for the regional, and zonal spatial scales. The net radiation should be determined for the equator to pole gradients and global spatial scales. Realization of these goals and the accuracies with which the components can be measured are a function of data interpretation and analysis (decomposition methods), orbital coverage and sampling (statistical significance), and instrument design (random plus bias errors).

The required minimum useful mission accuracies for monthly averages at the top of the atmosphere have been compiled from various scientific studies for the various spatial scales and are shown in Table 2.1

Table 2.1

Earth Radiation Budget Minimum Useful Accuracy Requirements

| Spacial Scale | Minimum Useful Requirement--$Wm^{-2}$ | | |
|---|---|---|---|
| | Longwave | Shortwave | Net |
| 250 x 250 Km Regions | ±14 | ±14 | |
| 1000 x 1000 Km Regions in Tropics | ±15 | ±15 | |
| $10^{o}$ Latitudinal Zones | ±12 | ±12 | |
| Equator to Pole Gradient | | | ±4 |
| Global | | | ±1 |

Innaccuracies associated with data interpretation and analysis, sampling, and instrument factors all have to be included in the error budget. From these mission requirements, the earth-viewing instrument uncertainty allocations have to be formulated. For wide field-of-view channels a requirement for a single sample uncertainty of ±4 $Wm^{-2}$ has been cited by Woerner and Cooper (1977). Included in the 4 $Wm^{-2}$ are a bias component of ±1 $Wm^{-2}$ and a random component of ±3.0 $Wm^{-2}$.

The overall mission requirement for the solar constant measurement is an accuracy of ±1.5 $Wm^{-2}$ with a reproducibility of ±0.3 $Wm^{-2}$. The design goal for a solar constant radiometer is an accuracy of ±0.1 percent of full scale (equivalent of ±1.37 $Wm^{-2}$) with a reproducibility of ±0.02 percent. Spectral measurements of the solar output have been requested by COSPAR WG6 (1978) and range from accuracies of 0.5% to 10% depending on the spectral region.

Further requirements are imposed on the earth-viewing systems if a "scanner" is used to delimit small measurement regions. Scanner data multiplied by influence coefficients from directional models are summed and averaged to provide monthly averages for the 250 by 250 Km regions. The noise equivalent radiance (NEN) requirements for shortwave and longwave channels are 1.00 $Wm^{-2}sr^{-1}$ and 0.13 $Wm^{-2}sr^{-1}$, respectively.

Most reports contain only the type of requirements discussion given above. However, during the last several years a great deal of effort has been expended on definition of Earth radiation budget requirements. The reader must realize by now that there are definitely multiple requirements to satisfy multiple scientific demands. Recent statements adapted from the U. S. program are included in Appendix A. The existence of the multiple requirements inherently complicates assessment of competitive measurement systems. On the other hand, we appreciate the broad spectrum of radiation budget data users!

NOTE: [When requirements are discussed (as in Appendix A) there is a tendency to forget that both instruments and measurements have properties -- and -- that they are not necessarily transferable. Thus, uncertainty, a measurement property is often improperly ascribed to an instrument. Or, precision and sensitivity, properties of instruments, are sometimes improperly used to describe measurements.]

In addition to the accuracy, and temporal and spatial scanning requirements, an Earth radiation budget measurement system has related lifetime and field-of-view requirements. It must perform in space for several years (ideally 3-5 years or longer) while yielding a stable data output. It is stressed that SIMPLICITY is the key for the achievement of a significant instrument lifetime.

Synopsis

Requirements for Earth Radiation Budget measurements are well defined. A timely measurement program should begin as soon as possible to be a part of new international climate initiatives. Because the science requirements emphasize long data periods of stable measurements, simple, reliable instrument systems are in demand. Alternate ways to measure radiation budget, using separate physical principles, would provide welcome scientific credibility to the overall climate data set.

## 3. OBJECTIVES OF THE PRESENT STUDY

The purpose of this study is to carry out a detailed comparison of two methods for measuring the Earth's radiation budget from space-borne sensors:

(a) A Radiometric Method

(b) A Radiation Pressure Method

The activities to be performed will include the following (section numbers indicated):

Basic Physics Principles (Section 4)

A comparison of the basic physics principles involved for each of the two techniques shall be performed, highlighting the fundamental differences between the two approaches.

Sensor Implementation (Section 5)

A review of (existing or potential) sensors for each technique will be performed including a comparison of instruments/sensors merits; a description of critical areas for each class of instruments will be performed in view of the mission requirements (long term measurements, accuracy of measurements, stability of sensors, space and time resolution, inflight calibration). Actual data from previous measurements will be used in the analysis.

Platform and Space System Requirements (Section 6)

The impact of sensors upon the platform and the space system will be identified and analysed. This analysis ranges from subsystems level (such as attitude measurement) up to the complete system level (sampling problems). Actual data and special sampling simulation will be used as needed.

Data Analysis Requirements (Section 7)

A comparison of the two techniques will be performed as far as data anlaysis on ground is concerned including special model requirements. Results from wide field-of-view flat and spherical measurement systems will be considered.

Possible Complementary Mission (Section 8)

During the course of the study it became apparent that the two separate methods of measurement be combined into a single system. Results from such a consideration are presented. It provides a third method.

Applicability of the Three Methods (Section 9)

The results obtained above will be discussed in view of the three major objectives of an Earth radiation budget study: solar constant, global budget and zonal/regional budget.

The comparison of three methods to measure the Earth's radiation budget will reflect the areas noted above. Wherever possible, we will cite examples from past measurements and/or computer simulations so the comparison is to be deeply rooted in the present state-of-the-art. Our comparison will show the need for additional tests of the three methods to provide information presently unavailable. We believe the

present study will aid the ordering these tests once form requirements and resources are identified by ESA.

Synposis

The objectives of the present study were specified by ESA after discussion with the authors. During the course of the work several new areas of inquiry were also examined.

# 4. PHYSICAL PRINCIPLES OF THE MEASUREMENT METHODS

## 4.1 Instrument Terminology

A classification of actinometric radiometers for measuring the various radiative components (irradiances) has been standardized by the WMO and is given by Coulson (1975). Although the terminology which has been adopted was directed primarily for ground and aircraft based instruments, it is conveniently extended to spaceborne platforms. The WMO classification indicates the type of measurement rather than the method of measurement and consists of the following:

| Instrument | Measurement |
|---|---|
| Pyrheliometer | Direct solar radiation at normal incidence (FOV subtends the solar point source) |
| Pyranometer | Hemispheric solar radiation ($2\pi$ sr FOV) |
| Pyrgeometer | Hemispheric terrestrial radiation ($2\pi$ sr FOV) |
| Pyrradiometer | Hemispheric total radiation ($2\pi$ sr FOV) |
| Net pyrradiometer | Upward and downward total radiation through a horizontal surface ($4\pi$ sr FOV) |

This classification applies strictly to the measurement of irradiant fluxes, not radiances; it does not restrict the band pass other than the bulk solar-terrestrial division (≃ 4 μm). In addition, in order to qualify as a flux instrument, the above class of instruments must essentially obey the cosine response function law.

Insofar as satellite platforms are concerned, the WMO classification is not strictly applicable because for Earth viewing sensors, wide angle FOV's are substituted for hemispheric FOV's such that (FOV$<2\pi$sr) in keeping with the treatment of the Earth disk as a "wide" point source. Wide angle viewing, rather than hemispheric viewing is required in order to eliminate stray radiative sources (sun, moon, satellite panels, etc.). However, it is convenient to retain the WMO classification. Because wide angle measurements represent basic components of any Earth radiation budget system, a separate discussion of them is given in Section 4.3. It must be stressed that wide angle satellite measurements represent irradiances at satellite altitude not at the top of the atmosphere.

In addition to the irradiance measurement instruments, there has been a wide range of instruments developed, particularly for but not limited to spacecraft, which measure collimated or limited FOV mean effective radiances. These would include such systems as the imaging telescopes developed for geosynchronous satellites (GOES, METEOSAT, GMS): the scanning radiometers used on the Nimbus 6 and 7 Earth Radiation Budget (ERB) instruments and proposed for the U. S. ERBSS and ESA SEOCS missions, and the high resolution imaging scanning radiometers flown on the NOAA and TIROS-N, operational satellites (SR, VHRR, AVHRR) and the U. S. Air Weather Service DMSP satellites. These instruments would also include ground and aircraft type systems such as the Barnes

PRT-5 and PRT-6 instruments for temperature sensing of the NESS Multi-scanning Radiometer (MSR); see Smith and Chen (1977). There apparently is no standard or easily adopted classification for the limited FOV instruments. It is worth noting, however, that an irradiance type instrument can be field stopped to achieve the limited FOV mode. In this case the cosine response characteristics can be maintained and exact mean effective radiances can be obtained. A separate discussion of ERB scanners is given in Section 4.4.

An important part of radiation budget studies is the spectral nature of the radiative components. This is particularly important for direct incoming solar radiation since the variability of the solar source is not uniform across the total solar band. Conventionally, the solar spectrum is divided into UV, visible, and near-IR components because each of these regions primarily influences particular components of the atmosphere's radiative dynamics (respectively upper atmospheric chemistry and heating, oceanic storage, tropospheric heating).

Again, there is no convenient classification of instruments which denotes spectral type measurements (of which there are a wide variety covering UV to microwave). This has led to a number of generic terms over the years, such as UV dosimeters, spectro-photometers, albedometers, spectro-pyroheliometers, and spectro-pyranometers. Although spectro-pyrheliometers and spectro-pyranometers are adequate definitions for spacecraft instrumentation, traditional terminology has simply been flux spectrometers for irradiance instruments and multi-spectral-radiometers for limited FOV instruments. The methodology used for the beam splitting (i.e., dichroics, gratings, prisms, chemical reactions, interference

filters, multiple aperatures, etc.) has not been used as a means to develop a standard classification scheme. In this study we will be as specific as possible when discussing limited FOV or narrow band instrumentation.

## 4.2 Radiometric Methods

There are two broad types of radiometeric detectors (Coulson, 1975; Hudson, 1969):

1. Thermal detectors
2. Photodetectors

Thermal detectors are based on the transformation of radiant energy to heat energy, giving rise to a temperature change in a selected receiver material. The temperature change is then registered according to various electronic or thermometric principles. For the purpose of this discussion we can classify the thermal detectors as follows:

1. Calorimeters
2. Thermocouples
3. Thermopiles - flat plate
4. Thermopiles - cavity
5. Metal bolometers
6. Semiconductor bolometers (thermisters)
7. Pyroelectric detectors

The calorimeter is a device in which temperature change of a heat absorbing substance (water, silver, metal strips, gas) is measured directly (thermometers, bimetallic elements, gas pressure). These instruments are relatively simple, with slow response characteristics, and generally not applicable to remote sensing applications.

The thermocouple is based on the Peltier effect; the production of an electromotive force (emf) across the junction of two dissimilar metals at different temperatures. Although a single thermocouple will not transduce or register a significant emf, a series configuration serves to amplify the electrical voltage needed to register an accurate measurement.

A thermopile is developed from the emf principle and consists of a series of thermocouple pairs operating on the basis that an N pair series produces N times the voltage of a single pair. The thermopile is the most frequently used detector in ground based radiometry and wide angle satellite based radiation budget measurements. Generally, the radiation receiver of a thermopile device will consist of a non-selective material; the radiative band pass is achieved by various types of cutoff and/or interference (band pass) filters and windows.

The basic components of a flatplate thermopile detector would then consist of a selective radiative window, a flat black-body receiver surface of known area and known absorptivity (near 1.0); a thermopile in direct contact with the receiver; and an electronics component needed to measure the voltage potential over the thermopile circuit. If the receiver behaved ideally, it would absorb all windowed radiation, would have equivalent response to equal amounts of radiative or electric power, and would not be affected by the actual registering components. In addition, for a true flux measurement, the detector must respond in proportion to the cosine angle between the radiation stream and the normal to the received area (cosine response function). Finally, if the receiver is truly non-selective, it will maintain a uniform spectral absorptivity response as the angular distribution of incoming intensity changes.

To achieve near ideal performance a class of instruments is now used in an attempt to minimize the above problems. These are the so-called cavity radiometers operated in the passive or active (self-calibrating/absolute) mode. The philosophy behind cavity radiometry is to literally trap photons in an enclosed cavity thus increasing the probability for absorptance[1] (minimizes the effect of surface coating degradation), and decreasing the potential for angular response variability. Since the compensating cavity radiometers of the electric substitution self-calibrating type are now used by the WMO as performance standards instruments, they will be considered in more detail (Section 4.5).

The thermopile most commonly used today, generates its own emf in proportion of the temperature change at a "hot" junction of two selected metals having a large difference in thermoelectric preperties. The temperature change is created when (earth) radiation varies upon the detector surface of area A, essentially upon the array of "hot" junctions. A reference level is obtained from the cold junctions connected to a large thermal mass shielded from variations in irradiance.

A typical thermopile of the type flown on Nimbus 6 and 7 and on Mariner 6 and 7 has the response expression:

$$\Delta E = E - E_o = \frac{\Delta CF}{S_o GS(T)V_a} \qquad (4.1)$$

---

[1] Recent tests at NBS (Geist, personal communication) have determined A = 0.9985.

where,

E is the irradiance ($Wm^{-2}$) at the channel aperture in an assigned spectral interval, e.g. 0.2 to 5 μm (pyranometer mode) or 0.2 to 50 μm (pyrradiometer mode),

$E_o$ is the apparent target irradiance ($Wm^{-2}$) caused by emissions of the thermopile and other optical components,

ΔC is the digitized channel output signal (bits) in counts (the difference in counts with the source exposed and with the aperture covered with a black plate at the detector temperature),

$S_o$ is the thermopile sensitivity ($VW^{-1}m^{2}$) in air at 25°C,

G is the channel electronic gain (bits · $V^{-1}$) at the thermopile,

S(T) is the ratio of the thermopile sensitivity at the pertinent temperature to its sensitivity at 25°C,

$V_a$ is the vacuum to air ratio (the ratio of the thermopile sensitivity in a vacuum to its sensitivity in air),

F is the filter factor and is the ratio of the total irradiance of the source in the assigned spectral interval ($\lambda_1$-$\lambda_2$) for each channel to the actual irradiance reading the detector:

$$F = \int_{\lambda_1}^{\lambda_2} E(\lambda)d\lambda \; / \; \int_{\lambda_1}^{\lambda_2} E(\lambda)\tau(\lambda)d\lambda \qquad (4.2)$$

where,

$E(\lambda)$ is the source spectral irradiance and $\tau(\lambda)$ is the spectral sensitivity function of the channel, i.e., primarily the transmission of the quartz window (Suprasil-W hemisphere). The thermopiles are assumed to be spectrally non-selective.

The conventional thermistor bolometer is based on the change of resistence of a metallic material. If two resistence elements are placed in a simple circuit (Wheatstone bridge) such that the first is exposed to the radiative source whereas the second is shaded (ambient conditions being similar) the temperature difference between them will generate an electric imbalance registered on a potentiometer.

This methodology led eventually to the semi and super conductor bolometers (superconductors are not considered here because of the near $0^{\circ}K$ temperature environments required). Semiconductors such as sintered manganese, cobalt, and nickel oxides demonstrated a remarkable improvement in bolometer technology (over metallic elements) because of their marked improvement in negative temperature coefficient of resistivity (> 4% per $^{\circ}C$). Rapid time response performance is easily achieved by fabrication of extremely thin flake elements. Although thermistors are no longer utilized directly for modern spacecraft irradiance measurements, they are still used to monitor cavity, optics, and various other instrument component temperatures for inflight calibration purposes.

The final category of thermal detectors and one of primary importance to modern satellite instrumentation is the pyroelectric detector. The operational principle at work for this type of detector is again based on heating, but in this case the temperature change effect induces crystal structure modification of the pyroelectric element. Pyroelectric crystals absorb heat which in turn leads to changes in the crystal lattic spacings, thus modifying the electric polarization of the crystal itself. This change of the electric field is in direct proportion to the rate of change of temperature and can be measured by placing the crystal in an electric circuit. Because of the differential response property, modulation of the radiative

source is required. This necessitates the use of radiation choppers, for purposes other than their standard application as optical modulators for unwanted signal suppression; see Hudson (1969). Although choppers can complicate the weight, power and mechanical requirements on a satellite, the fast response performances and the excellent sensitivity characteristics of pyroelectric detectors make them highly competitive with the photoconductive type detectors. Table 4.1 provides a list of pyroelectric materials and their associated properties. Of the high curie point materials, Lithium Tantalate provides the overall best performance. The scanner component of the ERB instruments, flown on Nimbus 6 and 7, includes such defocussed pyroelectric detectors, as does the scanner for the proposed ERB$S instrument, which has been accepted as the operational U.S. earth radiation budget instrument for the 1980's; see Smith et al. (1975), Jacobowitz et al. (1978), Vonder Haar and Wallschlaeger (1978).

Photodetectors are mostly frequency selective and operate on a fundamentally different principle than the heat activated detectors. In this case the individual collisions of photons, from the incoming radiation streams, onto the photodector element, give rise to the release of electrons and thus an electronic current. These detectors are characterized by extremely fast response times and high spectral sensitivity but do not provide an absolute measurement. It should be noted that the quantum efficiency of photodetectors is quite low (generally less than 10%) and the excess photons do give rise to heating of the material. Not surprisingly, the sensitivity of most of these materials is temperature dependent thus requiring some type of stabilizing thermal control for accurate measurements. Coulson (1975) provides a convenient classification and discussion:

TABLE 4.1

| Detector Material | Curie Temp. | Dielectric Constant | Pyroelec. Coeff. | Specific Heat | Loss Tangent | Ri(A/W) |
|---|---|---|---|---|---|---|
| | ($C^0$) | $\varepsilon$ | ($C\ cm^{-2}{}^0K^{-1}$) | ($J\ cm^{-3}{}^0K^{-1}$) | tan $\delta$ | $x10^{-6}$ |
| Lithium Tantalate | 660 | 47 | 1.9 | 3.16 | .005 | 2.0 |
| Lead Titanate | 470 | 200 | 6.0 | 3.36 | .01 | 5.95 |
| Lead Zirconate Titanate | 270 | 1800 | 2.0 | 3.3 | 0.2 | 2.22 |
| Lithium Niobate | 1210 | 30 | 0.4 | 2.8 | 001 | 0.05 |
| Lead Germinate | 177 | 60 | 1 | | | |
| Strontium Barium Niobate 50/50 | 115 | 380 | 6.5 | 2.1 | .01 to .02 | 10.0 |
| Tri-glycene Subplate | 49 * | 40 | 3.5 | 2.5 | $10^{-3}$ | 4.67 |
| Tri-glycene Selenate | 60 * | 34 | 5.4 | 2.5 | $2 \times 10^{-3}$ | 7.20 |

Pyroelectric Detector Materials

1. Photovoltaic detectors
2. Photoconductive detectors
3. Photodiode detectors
4. Photoemissive detectors

The photovoltaic detectors are essentially self-generating voltage response materials when exposed to shortwave radiation; the selenium cell is an example. Other materials such as indium antimonide, indium arsenide, and gallium arsenide can be used in this mode. Although photovoltaic elements are not generally applied to satellite based radiation measurements, they have found their way onto satellite platforms for power generation (e.g. the silicon solar cell), and as light meters for automatic gain adjustment units such as used for nighttime shortwave imaging on the DMSP type satellites.

A common satellite detector used for narrow-band near-infrared and infrared measurements is the photoconductor. These materials undergo electrical conductivity changes when exposed to radiation. They are generally required to perform at fairly low temperatures. Materials such as lead sulfide (PbS), lead selenide (PbSe), and mercury-cadmium-telluride (HgCdTe) are appropriate to this technology. For example, the infrared detectors on the SMS/GOES and GMS (Japanese geosynchronous satellite) Visible Infrared Spin Scan Radiometer (VISSR) instruments are HgCdTe elements. They are also found on spectrometer type instruments such as the proposed SEOCS scanning radiometer due to their high sensitivity over narrow band passes (See Hoffman, 1978). A wide selection of materials are available which generally cover a good portion of the most interesting regions of the terrestrial radiation spectrum. Table 4.2 from Coulson (1975) provides a brief list of photoconductive materials and their associates response

# TABLE 4.2

*Typical Values of Operating Parameters of Photoconductive Cells*[a]

| Detector material | Operating temperature (°K) | Spectral peak ($\mu$m) | Useful spectral range ($\mu$m) | Detectivity range $D^*$ (cm $Hz^{1/2}$ $W^{-1}$) |
|---|---|---|---|---|
| Lead sulfide | 295 | 2.4 | 1.0 to 3.0 | 0.7 to 1.5 × $10^{11}$ |
| Lead sulfide | 193 | 2.7 | 1.0 to 3.5 | 2.0 to 7.0 × $10^{11}$ |
| Lead sulfide | 77 | 3.2 | 1.0 to 4.0 | 0.8 to 2.0 × $10^{11}$ |
| Lead selenide | 295 | 3.7 | 1.0 to 4.5 | 0.3 to 1.2 × $10^{10}$ |
| Lead selenide | 193 | 4.4 | 1.0 to 5.1 | 1.5 to 4.0 × $10^{10}$ |
| Lead selenide | 77 | 5.0 | 1.0 to 6.5 | 1.0 to 3.0 × $10^{10}$ |
| Indium antimonide | 77 | 5.3 | 2.0 to 5.4 | 2.5 to 5.0 × $10^{10}$ |
| Germanium–gold | 77 | 5.0 | 2.0 to 7.0 | 3.0 to 6.0 × $10^{9}$ |
| Germanium–mercury | 28 | 11.0 | 2.0 to 13.8 | 0.7 to 1.5 × $10^{10}$ |
| Germanuim–cadmium | 21 | 22.0 | 2.0 to 23 | 0.7 to 1.5 × $10^{10}$ |
| Germanium–copper | 15 | 24.0 | 2.0 to 28 | 0.7 to 1.5 × $10^{10}$ |
| Germanium–zinc | 12 | 35.0 | 2.0 to 38 | 0.7 to 1.5 × $10^{10}$ |
| Mercury–cadmium–telluride | 77 | 12±1 | 8.0 to 13 | 2.0 to 6.0 × $10^{9}$ |

[a] As given by Bolz and Tuve (1973).

characteristics. Figure 4.1 (also from Coulson) provides a comparison of the spectral sensitivities of various photoconductive detectors to various thermal detectors.

The silicon photodiode is capable of operating in either a photoconductive mode or a photovoltaic mode depending on whether it is supplied a bias voltage. It has the advantage of not requiring cooling. Three of the ten diodes do not provide as fast response times as the photo multipliers, but they are able to operate at frequencies below the binding force frequency limits required by the photoemissive materials.

The photoemissive type detectors are activated in the same fashion as the photovoltaic and photoconductive materials but instead of the electrons remaining within the element and altering the voltage potential or conductive properties, they are ejected from the material and collected on a charged surface (anode), thus giving rise to the required electric current. An improvement of this basic design (the photomultiplier) is to accelerate the initial electron stream (in a vacuum) by a high intensity electric field toward a secondary target where in turn an even greater number of electrons are released, and thus an amplification of the detector sensitivity. This process is repeated until the desired sensitivity is achieved. Photomultiplier tubes may also be of the gas type, in which the freed electron stream serves to ionize the gas and yield order of magnitude increases sensitivity over the vacuum type systems. Gas type photomultipliers suffer, however, from shorter lifetimes and slower response characteristics.

An interesting aspect of the photoemissive materials (e.g. lithium, cesium) is that they provide their own near infrared cutoff, due to the

FIGURE 4.1

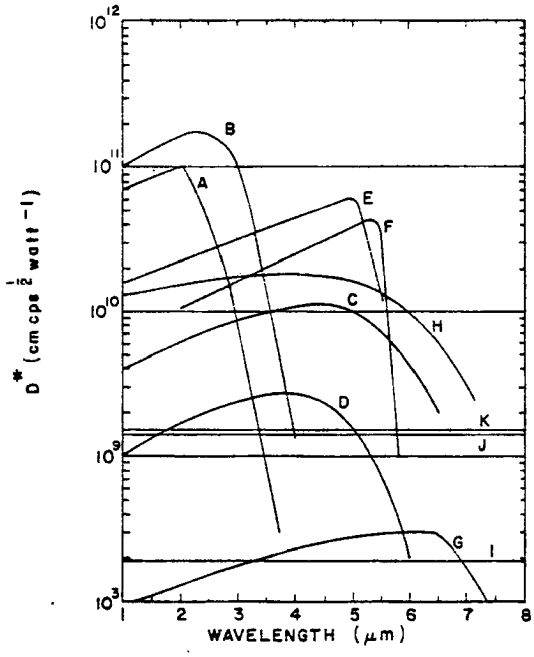


*Fig. 4.1.* Spectral sensitivity of various types of detectors, expressed in terms of $D^*$ (adapted from Brown, 1965). (A) Lead sulfide: 293°K; (B) lead sulfide: 195°K; (C) lead selenide: 77°K; (D) lead telluride: 77°K; (E) indium antimonide (photoconductive mode): 77°K; (F) indium antimonide (photovoltaic mode): 77°K; (G) indium antimonide (photoelectromagnetic mode): 293°K; (H) gold-doped germanium: 77°K; (I) thermistor bolometer; (J) thermocouple; (K) Golay cell.

binding forces required to release electrons. Einstein expressed the required relation as:

$$h\nu \geq e\phi \qquad (4.3)$$

where the photon energy $h\nu$ must overcome the binding energy $e\phi$ ($e \equiv$ unit electrical charge, $\phi$ the material work function). Most materials are not activated by wavelengths above 1.0 μm thus restricting the photomultiplier to the UV and visible part of the solar spectrum. Figure 4.2 from Coulson (1975) gives the sensitivity as a function of wavelength for a variety of photomultiplier tubes.

Photomultipliers were selected for the visible radiometers on the GOES and GMS type instruments (VISSR) because the rapid scan rate (100 rpm) of these satellites requires extremely fast detector responses. In these systems, light is focused by telescopic optics to separation prisms and then piped (via fiber optics) to an array of photomultipliers. In contrast the basic imaging systems used on the older NOAA operational satellites, i.e., the scanning radiometers (SR, VHRR) use thermister bolometers for the visible measurements.

4.2.1 Wide Field-Of-View Irradiance Instruments (Pyranometers, Pyrgeometers, Pyrradiometers)

Most climate requirements for Earth radiation budget measurements can be met by direct measurement of irradiant fluxes by spaceborne detectors. These fluxes are conveniently labeled $K\downarrow$ (shortwave incoming, $K\uparrow$ (shortwave emitted--0.2 - 4.0 μm), $L\uparrow$ (longwave emitted--4.0 - 100.0 μm), $Q\uparrow = K\downarrow + L\uparrow$ (net emitted), $Q^* = K\downarrow - Q\uparrow$ (net global radiation). These measurements represent the radiant sources or exitances, or a combination thereof, of the basic global components. The degree of representation of the Earth components is a function of inhomogeneity of the Earth fields,

FIGURE 4.2

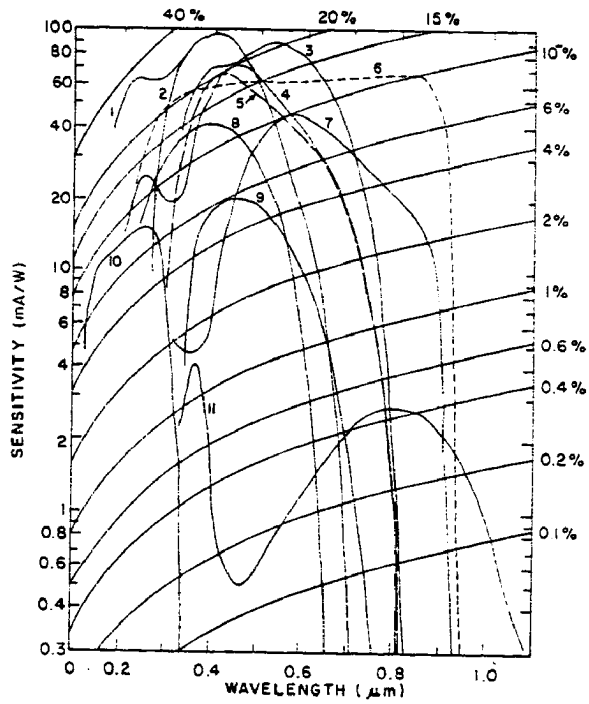


*Fig. 4.2.* Typical sensitivity as a function of wavelength for various types of photomultiplier tubes (from RCA Tech. Publ. No. PIT-700B, dated 12/71). Curve 1: K–Cs–Sb (133); curve 2: K–Cs–Sb (116); curve 3: Na–K–Cs–Sb (111); curve 4: Na–K–Cs–Sb (138); curve 5: Na–K–Cs–Sb (110: *S*-20); curve 6: GaAs (128); curve 7: Na–K–Cs–Sb (119); curve 8: Cs–Sb (102: *S*-4); curve 9: Ag–Bi–O–Cs (106: *S*-10); curve 10: LiF (125); curve 11: Ag–O–Cs (101: *S*-1).

content of the fields, and height of the satellite. These factors will be considered in the data analysis section for both methods under study. The basic principle for measurement of power (P) input to a perfectly absorbing, cosine response detector (flat black body) is denoted by:

$$P = \int_{\Omega} I\cos\theta d\Omega = \int_{0}^{2\pi}\int_{\theta_1}^{\theta_2} I(\theta,\phi)\cos\theta\sin\theta d\theta d\phi \qquad (4.4)$$

where,

$I(\theta,\phi)$ is the angularly dependent radiant intensity ($Wsr^{-1}$),

$\Omega$ is the solid angle subtended by the desired Earth field (normally the entire disk) with respect to the detector and defined as the detector field-of-view (FOV). It is composed of a zenith angle (angle between the radiation stream vector and the normal to the receiver) and an azimuth angle $\theta$.

The irradiance (E) is given by:

$$E = P/A \qquad (4.5)$$

where,

A is the area ($m^2$) of the detecting surface.

Note that if the surface of the radiometric detector is a sphere, $\cos\theta = 1$ at all times. Note also that E is determined at the satellite altitude and thus it is required to infer flux at the top of the atmosphere. Since $\Omega = A_e/r^2$ with $A_e$ the area of the Earth field and r the distance between Earth and the satellite detector, the measured irradiances from the same Earth field varies by $(1/r^2)$. Most wide field-of-view systems do not use optics to "gather more radiance"; their fields are limited by

stops that define an instantaneous geometric FOV. It generally extends from horizon to horizon and pole to pole, thus subtending a total angle of approximately $125^{\circ}$ at orbital altitudes near 1000 Km.

For a complete broad panel budget it is sufficient to determine $\alpha_r$ and any pair of K↑, L↑, Q↑, or Q* except the Q↑, Q* pair since:

$$\begin{aligned} Q\uparrow &= K\uparrow + L\uparrow \\ Q^* &= K\downarrow - Q\uparrow \end{aligned} \qquad (K\uparrow, L\uparrow \text{ known}) \qquad (4.6)$$

$$\begin{aligned} L\uparrow &= Q\uparrow - L\uparrow \\ Q^* &= K\downarrow - Q\uparrow \end{aligned} \qquad (K\uparrow, Q\uparrow \text{ known}) \qquad (4.7)$$

$$\begin{aligned} Q\uparrow &= K\downarrow - Q^* \\ L\uparrow &= Q\uparrow - K\uparrow \end{aligned} \qquad (K\uparrow, Q^* \text{ known}) \qquad (4.8)$$

$$\begin{aligned} K\uparrow &= Q\uparrow - L\uparrow \\ Q^* &= K\downarrow - Q\uparrow \end{aligned} \qquad (L\uparrow, Q\uparrow \text{ known}) \qquad (4.9)$$

$$\begin{aligned} Q\uparrow &= K\downarrow - Q^* \\ K\uparrow &= Q\uparrow - L\uparrow \end{aligned} \qquad (L\uparrow, Q^* \text{ known}) \qquad (4.10)$$

The measurement pair is optional but the solution is basically dictated by the achievable measurement accuracy. Broad band pyranometers are more applicable than pyrogeometers since highly accurate infrared windows are difficult to design or exceedingly expensive to manufacture. The standard shortwave window is a quartz hemisphere which has good longwave cutoff properties. Although all quartz domes are somewhat catacaustic, the grade III Suprasil-W fused silica hemispheres used on Nimbus ERB instruments and the planned ERBSS instrument indicate good square wave properties from 0.15 to 4.5 μm; see Figure 4.3 from Vonder Haar and Wallschlaeger (1978). Longwave windows such as prepared from diamond substrates can be fabricated for square wave type transmission, but cutoff at approximately 50 μm, thus eliminating $\approx$5% of the terrestrial infrared radiation. Simpler filters such as thalium bromide coatings do not provide good cutoff properties.

FIGURE 4.3

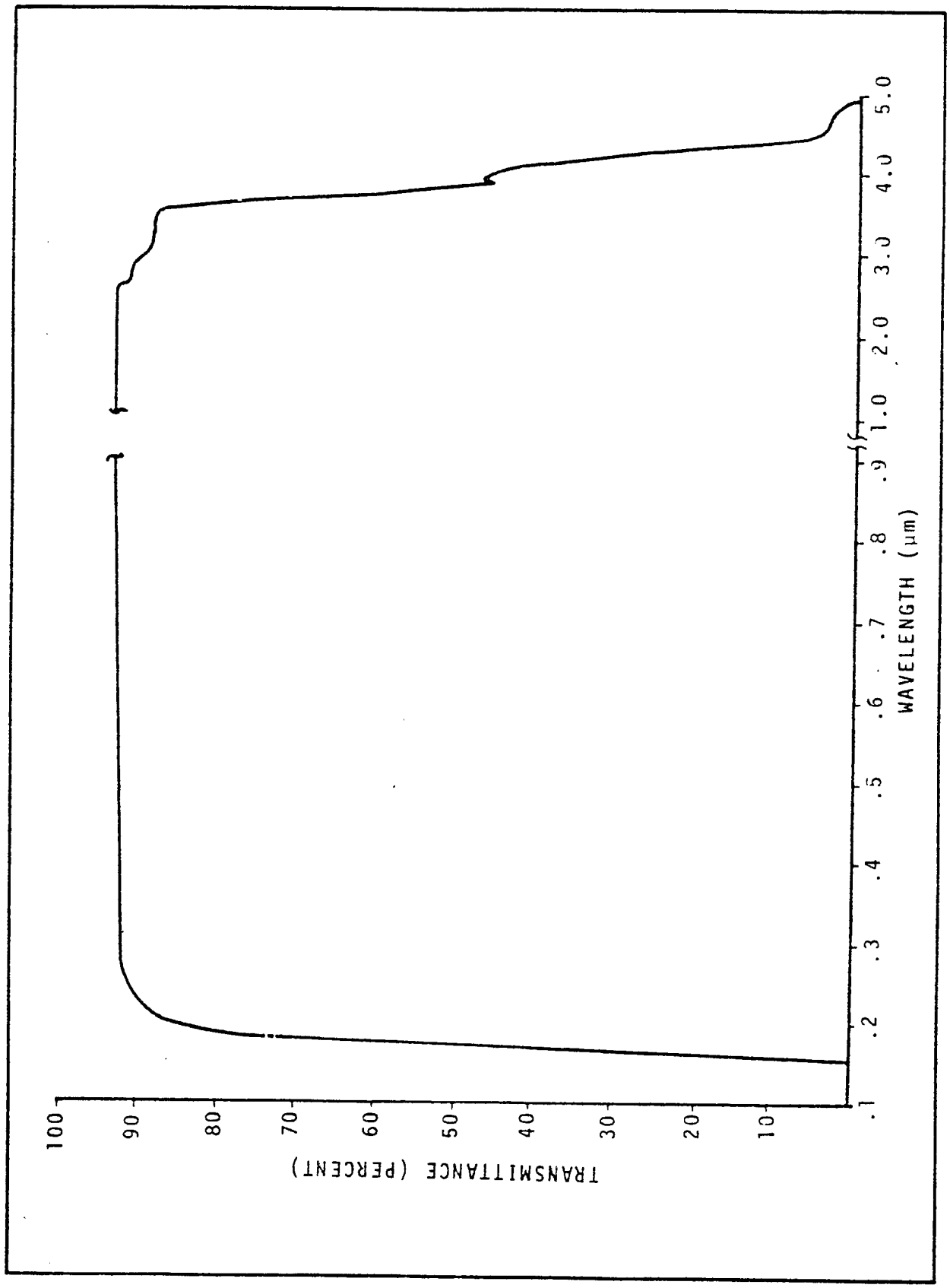


Transmittance of Suprasil-W (Thickness 2mm)

Since a Q↑ measurement requires no windows or filters, the simplest broad band budget system would include a pyroheliometer, pyranometer, and pyrradiometer.

Interference or band pass filters such as Schott glass shortwave filters or germanium substrate longwave domes are not germain to this report and will not be discussed.

4.2.2 Radiance Measurements from a Scanner

Certain scientific objectives require high areal specificity of the Earth radiation budget. Use of a small FOV to obtain these data is very analogous to the problem of imaging the Earth field from geo-synchronous satellite telescopes. However, radiation budget spectral bands are usually different from imaging bands (primarily shortwave and longwave windows) and generally conform to the broad regions noted in the previous section.

Orbital measurements of reflected and emitted radiation from e.g. 50 x 50 Km spots provide a determination of the total radiation budget over a spot via a measurement of the angularly dependent radiance (N), and an inference of the top of atmosphere irradiance E(x,y) from N (or combinations of N's); see Raschke et al. (1973). This can be expressed by:

$$E(x,y) = \int_0^{2\pi} \int_0^{\pi/2} N(\theta_\odot, \theta_s, \phi_r) X(\theta_\odot, \theta, \phi) \cos\theta \sin\theta d\theta d\phi \qquad (4.11)$$

where,

E(x,y) is the integrated flux corresponding to a position x,y on the sphere extending to the top of the atmosphere,

$N(\theta_o, \theta_s, \phi_r)$ is an angularly dependent radiance,

$\chi(\theta_o,\theta_s,\phi)$ is the bi-directional reflectance function of solar zenith angle ($\theta_o$), satellite zenith angle ($\theta_s$), and relative azimuth angle ($\phi_r$) in the plane tangent to the sphere centered at the earth and intersecting (x,y).

The more general deconvolution problem of determining radiative fluxes at the top of the atmosphere from wide angle, high altitude satellite platforms is discussed in Section 7.

Obviously, if the bi-directional reflection coefficients are unknown or approximately with some uncertainty, the determination of a directional reflectance (R) is known only within some uncertainty limit. R is defined:

$$R(x,y) = \int_0^{2\pi}\int_0^{\pi/2} N(\theta_\odot,\theta_s,\phi_r)\,\chi(\theta_o,\theta\ ,\phi\ )H^{-1}\sin\theta d\theta d\phi \qquad (4.12)$$

where,

H is the solar constant.

In addition, the albedo (A) suffers from this uncertainty and since:

$$A = \int_{t_1}^{t_2} H(t)R(x,y,t)dt \Big/ \int_{t_1}^{t_2} H(t) \qquad (4.13)$$

and if only one or several measurements are available for time integration, there is a further sampling uncertainty. These are the so called flux model problems discussed in various references.

Thus, while the physical principles of scanner measurements are clear, the inability to measure from a wide variety of narrow angles, coupled with our limited knowledge of the aniostropic reflectance and emittance by land and cloud fields, there is a practical measurement problem in attempting to acquire highly areal specific radiation budget data.

The actual detectors used in the scanners may range, as noted previously, over a variety of pyroelectric, photoemissive and photoconductive detectors. In general, each detector system can be rated by its Noise Equivalent Radiance (NEN). A standard expression of the characteristics affecting noise:

$$NEN = \frac{(NEP)(\Delta F)^{\frac{1}{2}} Ke}{Ao\Omega\varepsilon_o Km} \qquad (4.14)$$

where,

NEP is the detector's noise equivalent power,

$\Delta F$ is the noise equivalent bandwidth and is equal to 0.5 Ts, where Ts is the integration time,

Ke is an electronics noise factor,

Ao is the collecting area of the detector,

$\Omega$ is the solid angle field-of-view,

$\varepsilon_o$ is the effective optical efficiency for the detector system

Km is chopping factor for conversion from a peak to peak to rms signal.

4.2.3 Cavity Detectors for Measurement of Direct Solar Irradiance

In recent years a new class of radiometers has become available for field measurements. These are the so-called absolute cavity radiometers. The "new" Cavity Radiometer World Radiometric Reference (WRR) Scale at WRC-Davos, has taken a place along side the pre-existing International Pyrheliometric Scale IPS-1956 (to which it is referenced) and such radiometric scales as that used by The National Bureau of Standards (NBS). Absolute calibrations are now referred to an approved set of WMO instruments consisting of the following:

1. PACRAD
2. CROM
3. ACR
4. PMO

This group of instruments coincides with the Solar Constant Reference Scale -- See Brusa, Gillham and Crommelynek (1977). Several candidate radiometers for satellite applications are given below:

1. Eclectic Satellite Pyrheliometer (ESP) developed by J. Hickey of Eppley Labs
2. Active Cavity Radiometer (ACR-IV) developed by R. Willson of JPL
3. Primary Absolute Cavity Radiometer (PACRAD) developed by J. Kendall of JPL
4. PMO developed by Frohlich and Brusa of Physikalisch -- Meteorologisches Observatorium (PMO), Davos, Switzerland
5. CROM developed by Crommelynch of Institut Royal Meteorologigue de Belgique, Brussels
6. A High Speed Active Cavity Radiometer (HSACR) approach was studied by the University of Wisconsin

From a space measurement point of view they offer potential for highly accurate, longlife data, primarily because their "cavity" design maximizes detector absorptance and minimizes angular dependence, and because of their compensation mode self-calibrating characteristics. Presently, the first successful satellite cavity radiometer experiment is being carried on the Nimbus 7 satellite. The radiometer is of the Eppley/Gulton type, schematically shown in Figure 4.4. For earth radiation budget purposes, there is still a question if the more complex cavities

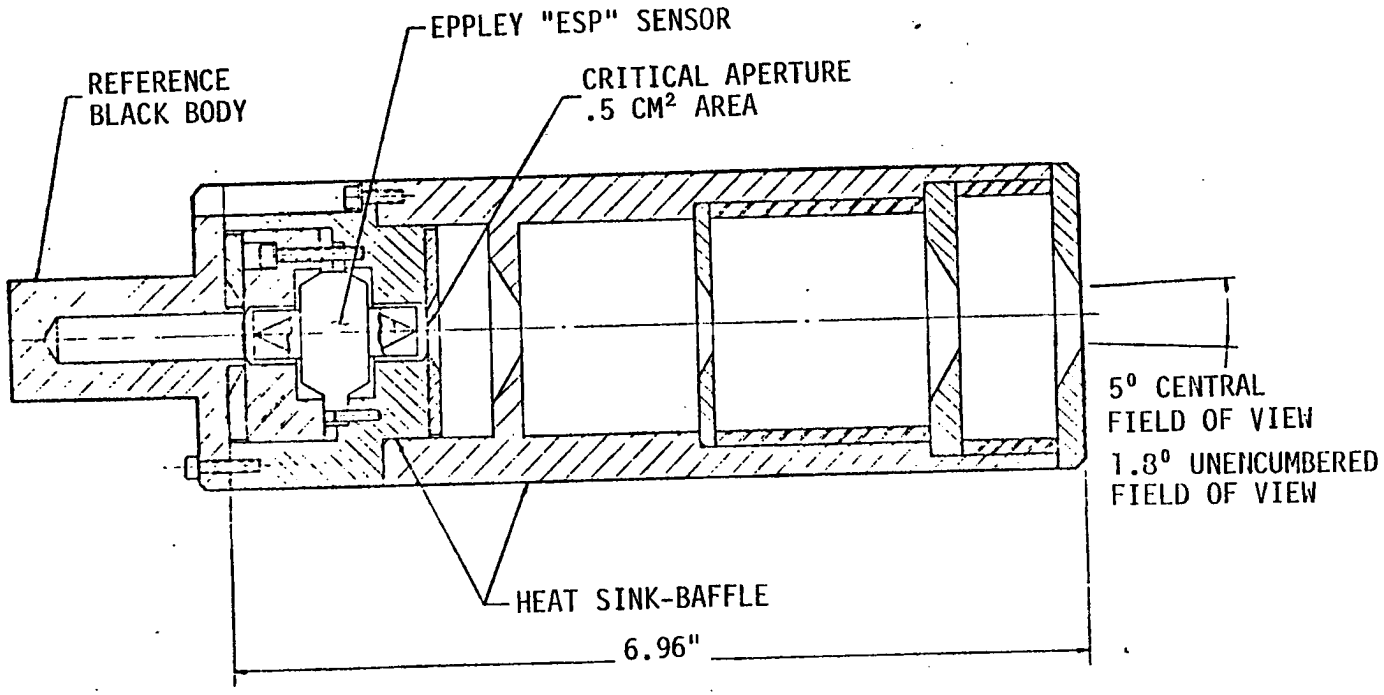


FIGURE 4.4

Schematic Drawing of Eppley-Gulton ESP

can withstand the trauma of launch and longtime space operations, and whether their response time will be fast enough to measure the changing Earth fields. Gulton Industries of Albuquerque, New Mexico estimates the Nimbus-7 cavity response time (channel 10C) as approximately one second.

The basic principles of operation of cavity radiometers are given by a discussion from Vonder Haar and Wallschlaeger (1978) and stem from a design review for the ERBSS instrument.

The advantages of the cavity detectors over the flat plate detectors are:

1. Improved receiver absorptance (hence better longwave response, and less sensitivity to coating degradation.
2. The cavities can be calibrated electrically. Flat plate receivers may also incorporate this feature.

The disadvantages of the cavity detectors are:

1. Volume
2. Weight
3. Power (depends on mode of operation)
4. Time constant and
5. A shutter may be required

The ACR-IV cavity radiometer made by JPL is generally operated in the active mode, i.e., the irradiance incident on the primary cavity is proportional to the difference in the electrical power applied to the secondary and primary cavities. The applied electrical power maintains a constant heat flow from each cavity to the housing or heat sink. With the shutter closed, both primary and secondary cavities are exposed to about the same irradiance and the power difference is minimized. With the shutter open,

the scene irradiance incident on the primary cavity reduces the electrical heat on that cavity necessary to maintain the constant heat flow to the housing. The change in the primary cavity electrical power is then proportional to the incident irradiance. In the passive mode, nickel resistance sensors measure the temperature difference between the two cavities; that difference being proportional to the incoming scene irradiance.

The ESP (Eclectic Satellite Pyrheliometer) of Eppley/Gulton employs a toroidal wire-wound thermopile, nearly identical to the flat plate thermopile receiver, to measure the temperature difference between the two cavities. In the active mode, heat is applied to the secondary cavity to null the thermopile output. Eppley feels no shutter is necessary as the thermopile sensor is both linear and sensitive over three decades and can measure very small temperature differences.

Because of the better absorptance of the cavities, the spectral response is essentially flat to beyond 50 micrometers. This is not true of the flat disc receiver which has increased reflectance at longer wavelengths regardless of the coating used. The electrical calibration feature of the cavities allows additional calibration points when rotated to look at space, regardless of the mode of operation. A Langley funded study is now underway at JPL to determine the potential for cavity detectors to operate in a wide field mode. Testing of a cavity detector with a wide field view limiter was performed at JPL by Kendall in 1977. These tests show a response slightly above a cosine response which was probably caused by scattering in the view limiter that was used.

In its simplest form, the thermopile detector may be considered as a two terminal device whose output is a voltage proportional to the difference in irradiances incident on the detector active receiver and reference

receiver surfaces. Internally, it may be considered as an array of thermocouples. It is constructed by wrapping a coil of constantan wire around an aluminum heat sink where a portion of the constantan wire is copper plated to form the thermocouples. Incident radiation is absorbed in a blackened 0.25-inch (6.35 mm) diameter disc-shaped receiver surface, changing its temperature, and in turn, generating a proportional net output voltage from the thermocouple array.

It is to be emphasized that this type of detector is now in use, with proven performance, in the Earth Radiation Budget (ERB) experiment aboard Nimbus-6. The ERB Solar Channel 3, which consists of a thermopile detector exposed to the sun all of the time, has exhibited no significant degradation after two years in orbit ($< \pm 0.1\%$). Toroidal wire-wound thermopiles with approximately the desired area have been made for use on the ESP, a version of which is included as one of the channels of the Nimbus-7 ERB (see section 5).

Tests performed on the ESP with irradiance levels up to 1.2 solar constants showed a temperature change of less than $1^{o}C$ and linear response over three decades. The toroidal configuration provides a highly uniform response over the disc receiver. This type of thermopile detector has a balanced reference receiver with the heat sink between the active and reference receivers. This balance and heat sinking technique minimizes the effect of any conductive thermal transients and allows a relatively fast time constant. The temperature difference, $\Delta T$, between the active and refernece receivers, is not allowed to reach high values for high incident flux levels, reducing the effects of temperature dependent responsivity nonlinearities. The desirable qualities of wire-wound thermopiles are good linearity, low temperature coefficient, long-term stability, and structural integrity. It should be noted that, for off-normal axis image points, the

detector presents a cross-section which varies as the cosine of the off-axis angle. Hence, the circular wire-wound thermopile detector is said to have a cosine response characteristic.

While exact data are not available, estimates have been made of the weight and power increases associated with the use of cavity radiometers rather than the flat plate thermopile. Without a shutter, the weight of each channel with increase by 0.395 kg or 0.87 lbs. This estimate is based on use of 90 percent of the available volume by a material with the density of aluminum. The available volume is a cylinder of 5.7 cm diameter and 6.35 cm height and a volume of 162.6 $cm^3$. If the cavity detector can be operated in the passive mode, there is no need for additional power over that already allocated per channel. In the active mode, it is estimated that each cavity channel will require approximately 0.5 watts. Use of cavity detectors in four Earth-looking channels would require an additional 1.58 kg or 3.48 lbs in weight and up to 2.0 watts of power.

Since shortwave channels do not require spectral response past 5.0 micrometers, a good compromise might be the use of passive cavity detectors for the total channels and the flat plate thermopile for the shortwave channels. This would increase the weight by 0.79 kg and not affect the power.

## 4.3 Radiation Pressure Method

The use of radiation pressure for the measurement of radiative flux begins with the Einstein mass-energy conservation principle:

$$E = mc^2 \tag{4.1}$$

which can also be expressed for a single photon hν:

$$Ec^{-1} = mc \tag{4.2}$$

and thus for a single photon ($h\nu$):

$$h\nu c^{-1} = mc \tag{4.3}$$

thus revealing the equivalence between photon energy and momentum. When this momentum is imparted to a secondary object (particle) of mass (M), conservation principles require the resultant force to produce an acceleration.

Van de Hulst (1957) expresses this transfer with respect to an extinction cross-section of the exposed particle:

$$\bar{M}_r \propto C_{ext} \tag{4.4}$$

where,

$\bar{M}_r$ is the momentum removed from a radiative beam and transferred to a particle, and

$C_{ext}$ is the extinction cross-section defined as:

$$C_{ext} = C_{abs} + C_{sca} \tag{4.5}$$

where,

$C_{abs}$ ≡ absorption cross-section,

$C_{sca}$ ≡ scattering cross-section,

and is a function of complex index of refraction, particle orientation, and the polarization of the incident beam.

For perfect absorbers $C_{ext} = C_{sca}$. If we define the actual cross-section C, then $(1 - C_{ext} / C)$ defines the transmissivity of the particle. When treating radiation pressure systems such as the D5B (CASTOR) Satellite or the proposed BIRAMIS system (see Tessier, 1977 and Onera, 1978), the effective extinction cross-section efficiency is 1.0 and thus the transmissivity is 0.0. This property need not hold, however, and leads to

rather interesting speculation concerning partially transparent satellites designed for band pass measurements. The $\bar{M}_r$ momentum imparted to the exposed particle represents a force exerted in the direction of propagation of the incident beam and results in radiation pressure.

If we consider grazing incidence on a particle surface where $\theta$ is the angle between the incident beam and the normal to the particle surface, $\bar{M}_r$ must be modified according to $\cos\theta$, resulting in:

$$M_r' \propto C_{ext}' = C_{ext} - (1 - \cos\theta)C_{sca} \qquad (4.6)$$

for absorbing particles, and:

$$M_r' \propto C_{ext}' = C_{ext}(\cos\theta) \qquad (4.7)$$

for non-absorbing particles. The resultant vector force ($\vec{F}$) on a particle of mass (M) by a radiative flux ($W_o$) is thus

$$\vec{F} = M\vec{a} = C_{ext}' \cdot (W_o\vec{c}^{-1}) \qquad (4.8)$$

and the acceleration ($\vec{a}$) is thus:

$$\vec{a} = (C_{ext}' \cdot M^{-1}) \cdot (W_o \cdot \vec{c}^{-1}) \qquad (4.9)$$

where we define $W_o\bar{c}^{-1}$ as the radiation pressure.

If we extend this principle to a sphere of radius (r), and considering the integral properties of a sphere we can define the effective cross-section.

We first define the following:

$A \equiv$ Absorptivity of the coating

$R \equiv$ Total reflectivity of the coating

$R_s \equiv$ Specular reflectivity component (4.10)

$R_d \equiv$ Diffuse reflectivity component

$T \equiv$ Transmisivity of coating (zero)

$\varepsilon \equiv$ Emissivity of coating

The following relationships apply:

$$A + R = 1.0 \text{ since } T = 0.0$$
$$R_s + R_j = R \tag{4.11}$$
$$\varepsilon \leq A$$

We assume that $R_d$ and $\varepsilon$ are representative of perfectly diffuse processes (or nearly so). Significant departures from isotropy will generally lead to errors in the measurements. We now define the effective absorption cross-section $\sigma_A$. All absorbed photons parallel to a direction $\hat{n}$ along paths designated by $\hat{u}$ provide a composite initial impulse force proportional to $\sigma_A$, where

$$\begin{aligned} F_A\hat{n} &= (W_o c^{-1})A dg\cos\theta\hat{u} \qquad (4.12)\\ &= (W_o c^{-1})A \int_o^{2\pi}\int_o^{\pi/2} \cos\theta r^2 \sin\theta d\theta d\phi\hat{u}\\ &= (W_o c^{-1}) \cdot A \cdot (\pi r^2)\hat{n}\\ &= (W_o c^{-1}) \cdot \sigma_A\hat{n} \end{aligned}$$

where $\sigma_A = (\pi r^2) \cdot A$ and $\theta$ defines the angle between $\hat{n}$ and the vector from the center of the sphere to the incident point at the surface of the sphere. Note that this angle serves as the declination angle component of the solid

angle integration. Note also that both transverse forces (normal to $\hat{n}$) integrate to zero since they symmetrically oppose for any selection of orthogonal axes.

Reflecting energy also leads to impulse forces. Specular reflection imparts incident impulses and reflecting impulses. As in the absorption case, the transverse forces cancel and we consider only the components parallel to $\hat{n}$. The incidence impulse is proportional to cosθ as is the reflecting impulse. In addition, the component of the reflection force parallel to $\hat{n}$ is proportional to cos2θ as seen in the following diagram.

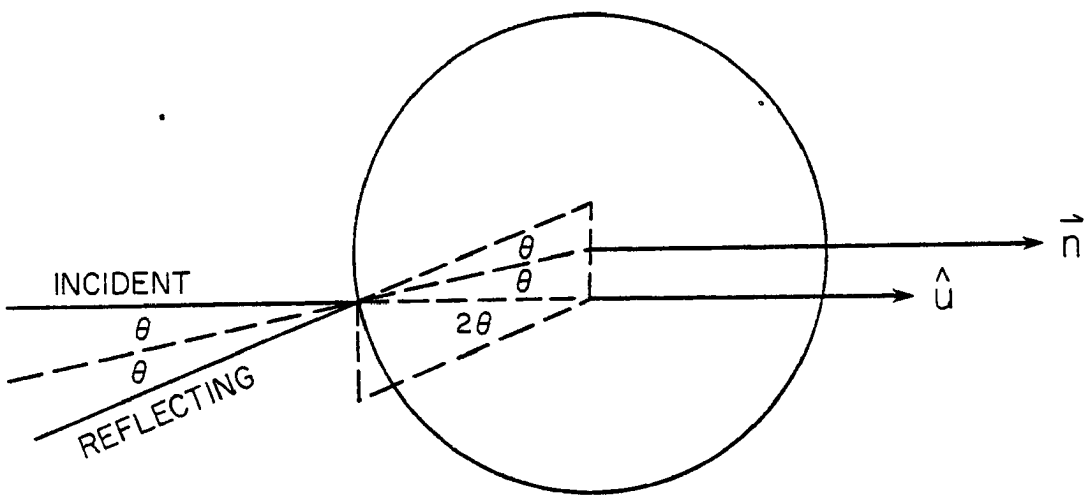

The integral form needed to determine the specular cross-section $\sigma_{R_s}$ is:

$$F_{R_s}\hat{n} = (W_o c^{-1})R_s ds\cos\theta[1 + \cos 2\theta]\hat{u} \qquad (4.13)$$

$$(W_o c^{-1})R_s \int_0^{2\pi}\int_0^{\pi/2} \cos\theta[1 + \cos 2\theta]r^2 \sin\theta d\theta d\phi\hat{u}$$

Using the double angle identify for cos2θ:

$$F\hat{n} = (W_o c^{-1})R_s \int_0^{2\pi} \cos\theta[2\cos^2\theta]r^2 \sin\theta d\theta d\phi\hat{u} \qquad (4.14)$$

Note that an impulse force along a radial vector $\hat{r}$ is proportional to $2\cos^2\theta$ and its component along $\hat{n}$ is $\cos\theta[2\cos^2\theta]$. Integrating either 4.13 or 4.14 yields:

$$F_{R_s} n = (W_o c^{-1}) \cdot R_s \cdot (\pi r^2)\hat{n} \qquad (4.15)$$

$$= (W_o c^{-1}) \cdot \sigma_{R_s}\hat{n}$$

where,

$$\sigma_{R_s} = (\pi r^2) \cdot R_s$$

Treating the diffuse reflection case, both the incident and reflection impulses are proportional to cosθ. The reflection impulse, however, involves a hemispheric integration, symmetric about the normal to a radial vector extended to the point of incidence. If we consider only perfectly diffuse reflection, we can determine a particular diffuse reflection pressure ($P_{R_d}$) with respect to the radial direction:

$$P_{R_d} = (W_o c^{-1})\cos\theta \int_0^{2\pi} \int_0^{\pi/2} \frac{R_d}{2\pi}\cos\theta' \sin\theta' d\theta' d\phi' \qquad (4.16)$$

where we note that $R_d/2\pi$ represents the weighting of $R_d$ for a particular direction over the $2\pi$ sr hemisphere of reflection and $(\theta',\phi')$ represent the angular quantities describing the hemisphere of reflection. This integral yields

$$R_{R_d} = (W_o c^{-1}) \cdot R_d \cdot \frac{\cos\theta}{2} \tag{4.17}$$

Considering the projection of this impulse in the $\hat{n}$ direction and integrating over $2\pi$ sr for both incident and reflection processes yields:

$$\begin{aligned} F_{R_d}\hat{n} &= (W_o c^{-1}) \cdot R_d \, ds \cos\theta[1 + \cos\theta/2]\hat{u} \qquad (4.18)\\ &= (W_o c^{-1}) \cdot R_d \int_0^{2\pi} \int_0^{\pi/2} \cos\theta \, [1 + \cos\theta/2] r^2 \sin\theta d\theta d\phi \hat{u} \\ &= (W_o c^{-1}) \cdot R_d \cdot \pi r^2 \left\{ 1 + \int_0^{\pi/2} \cos^2\theta \sin\theta d\theta \right\} \hat{u} \end{aligned}$$

The later integral expression yields 1/3, thus:

$$\begin{aligned} F_{R_d}\hat{n} &= (W_o c^{-1}) \cdot R_d \cdot (4/3\pi r^2) \qquad (4.19)\\ &= (W_o c^{-1}) \cdot \sigma_{R_d} \end{aligned}$$

where,

$$\sigma_{R_d} = (4/3 \, \pi r^2) \cdot R_d$$

Similarly, considering diffuse emission we find:

$$\begin{aligned} F_\varepsilon \hat{n} &= (W_o c^{-1}) \cdot \varepsilon \cdot (1/3 \, \pi r^2) \qquad (4.20)\\ &= (W_o c^{-1}) \cdot \sigma_\varepsilon \end{aligned}$$

where,

$$\sigma_\varepsilon = (1/3\ \pi r^2) \cdot \varepsilon$$ which does not represent a source term, rather a parasitic term.

Thus, the total source referenced cross-section ($\sigma$) is given by:

$$\sigma = \pi r^2[A + R_s + R_d + R_d/3] \qquad (4.21)$$

$$= \pi r^2\ [1 + (R_d/3)]$$

$$= \Sigma \cdot K$$

where we define K as the coating property coefficient and $\Sigma$ as the actual cross-section of the spherical receiver. The acceleration term along $\hat{n}$ is

$$a\hat{n} = SW_o c^{-1}\hat{n}$$

where $S = K \cdot \Sigma / M$ which we define as the sensitivity coefficient of the receiver; see Girard (1978) and Levadon (1978) for discussions. Note that spectral dependence is not considered here; spectral dependence in the diffuse reflection term must be minimized to avoid measurement uncertainty. The degree of polarization of the radiative source does not affect the measurement (see Mainguy et al., 1978).

We now consider all angular radiative sources $W_o(\theta,\phi)$ and the resultant acceleration component along an arbitrary (nominal) x' axis.

$$\vec{a}_{x'} = Sc^{-1} \int_0^{2\pi} \int_0^{\pi} W_o(\theta,\phi)\cos\theta\sin\theta d\theta d\phi x' \qquad (4.22)$$

Clearly, if $W_o(\theta,\phi)$ is constant for all $(\theta,\phi)$ then $\vec{a}_{x'} = 0$. Considering the basic sources (solar, terrestrial, lunar), there will be non-zero accelerations along x' and associated orthogonal components y' and z'. The summation of acceleration components yields the effective radiation pressure induced

acceleration a along a path $\hat{N}$. Since the integral quantity in 4.22 represents the net flux W, we say finally that the vectorial irradiance term W is given by

$$W = \vec{a} \cdot c/S \qquad (4.23)$$

An absorbing-reflecting-emitting sphere thus placed in a drag-free radiative environment will undergo an acceleration (a) along a path (N); see Pastre and Julliet (1977) and Barlier et al. (1978). If we define this acceleration vector ($\vec{a}$) as ($a'_x$, $a'_y$, $a'_z$) in some arbitrary nominal coordinate system, we have a means by radiation pressure to determine an equivalent flat-plate flux on a spherical receiver whose radiometric response function would be 1.0.

Since the properties of the acceleration vector are conserved under a coordinate transformation, we can rotate the arbitrary coordinate system to an (x,y,r) inertial coordinate system in which the r-axis extends radially from Earth center to the satellite, the y-axis parallel to the Earth spin axis, and the x-axis being the associated cross product in a right handed sense. We now have an acceleration vector component $a_r$ such that

$$W = (a_r \cdot c)S^{-1} \qquad (4.24)$$

where W is the same net radiative flux that would be measured at any point by a $4\pi$ sr flat plate net pyrradiometer at equivalent satellite altitude assuming error-free conditions. This is an intriguing feature of the radiation pressure measurement, i.e., it represents a fully integrated value of net radiation. Accordingly, the area-mass-coating sensitivity factor (S) serves as the control parameter for measurement accuracy; see Duhumel and Marchal (1978) and Mainguy et al. (1979) for detailed discussions.

The measurement of actual radiation components ($K\downarrow$, $K\uparrow$, $L\uparrow$, $Q\uparrow$, $Q^*$) from a spherical radiation pressure satellite is a 5-part problem:

1. Skin coating or transfer frunction properties
2. Measurement of acceleration
3. Removal of parasitic forces
4. Decomposing radiative induced accelerations into irradient fluxes at the satellite
5. Deconvolution of the satellite fluxes to top of atmosphere fluxes

Because the problems indicated in Part 5 are inherrent in any wide angle measurement (radiometric or radiation pressure) they will be discussed separately in Section 7.

Since the integrated response of a sphere is equivalent for perfectly absorbing or perfectly reflecting (specular) skin properties, it seems reasonable to select a coating which yields the fewest degradation problems. Fortunately, uniform degradation of the coating will not immediately lead to useless measurements. Some of these problems are addressed during the LZEEBE studies, e.g., see LARC (1975), and are under study for BIRAMIS; see Girard (1978).

The measurement of acceleration itself is a technical problem in electrostatics. The CACTUS (Capteur Accelerometrique Capaetif Triaxial Ultrasensible) instrument suspends a rhodium-platinum proof mass (4 cm diameter ball) within a 4.017 cm diameter cavity with 3 pairs of "forcing electrodes"; see Bernard et al. (1977). Figure 4.5 from Berhard et al. illustrates the CACTUS schematically. Accuracy of measurements depends critically on the centering and symmetry of the cavity. The ambient radiation forces and parasitic forces lead to displacement of the satellite with respect to the ball. This

FIGURE 4.5

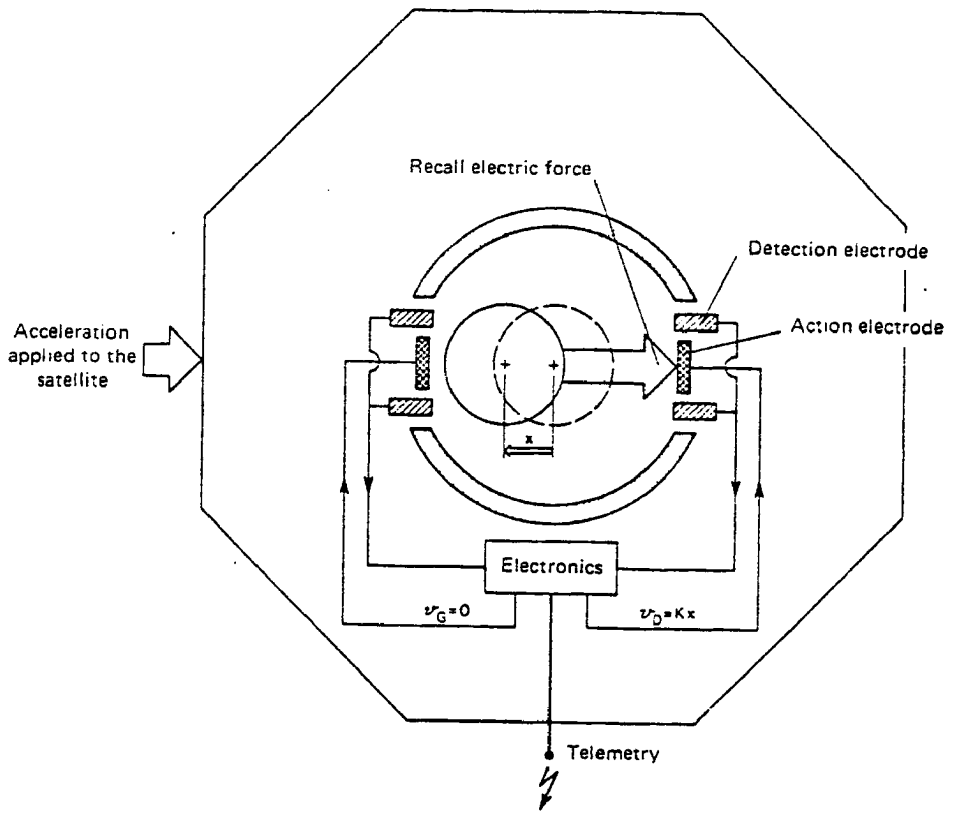


*Principle of the accelerometer.*

displacement results in capacitence changes along the axes of the accelerometer. The change in voltage potentials determined by 3 pairs of "detection electrodes" results in being able to monitor instantaneous orthogonal values of acceleration of the satellite. The combination of forces also leads to torques or twisting forces leading to spin. If the time constant of the accelerometer is much greater than the spin time constant, these torques are insignificant. Furthermore, controlled spinning is nominally required to overcome inertial forces, to minimize thermal gradients and to maximize attitude stability.

The parasitic forces affecting accelerometer measurements can be classified as external forces, and satellite or accelerometer induced forces. These are given by Mainguy (1978); see Figure 4.6 for an illustration from Bernard et al. (1977) and include:

External Forces:

1. Atmospheric drag
2. Lunar fluxes (reflected and emitted)
3. Solar wind (free protons)

Satellite and Accelerometer Induced Forces

1. Photonic thrusts (due to temperature gradients along the coating or internally)
2. Lorentz forces
   a) Charges on the satellite
   b) Charges on the ball
3. Inertial accelerations (ball mass center does not correspond to satellite mass center)

FIGURE 4.6

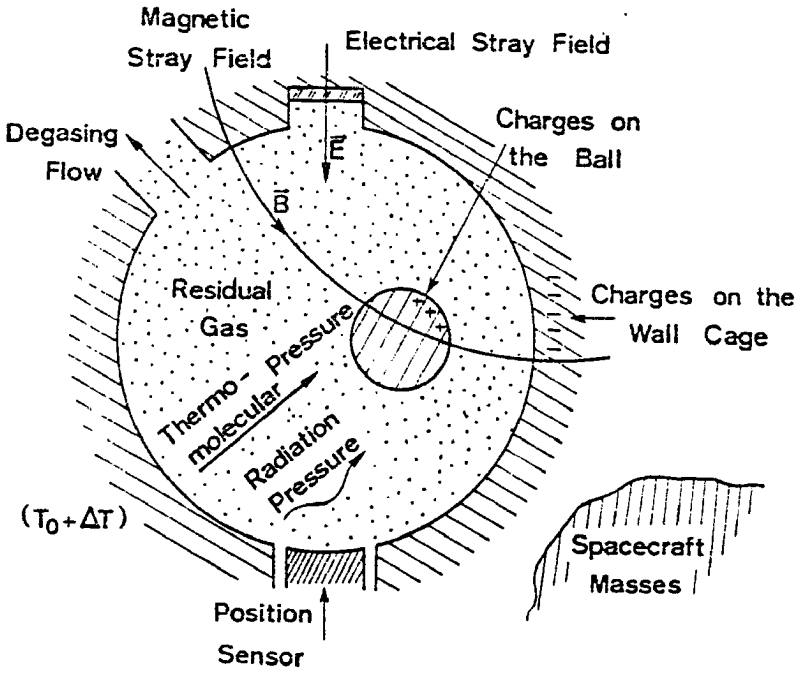


*Disturbing forces.*

4. Gravitational forces
   a) Gravity field gradient
   b) Mass attraction
5. Magnetic field forces
6. Residual gas forces in the cavity

All of these parasitic forces can be completely or partially overcome by various strategies.

Atmospheric drag forces are eliminated by going to high orbital altitudes (> 1000 Km). The charge buildup forces can be minimized by bringing the ball in contact with the accelerometer cage periodically. Photonic forces may be the most difficult to treat although the acceleration levels associated with them are fairly low. Most of the other forces are not serious and are explicitly discussed by Mainguy (1978).

The extraction of radiation components from the acceleration vector has two sources of geometric error. First of all, there are errors associated with the rotation of the accelerometer coordinate system due to uncertainties in the attitude. This simply places a condition on the accuracy of the attitude determination. Uncertainty in the attitude measurements translates to errors (directly proportional to the cosine of attitude angle uncertainties) along the flux or radial axis during the coordinate rotation (see Mainguy et al., 1978). A second, more serious geometric error, results from the displacement of the nominal z-axis from the inertial radial or r-axis. Since this relationship is constantly varying, due to satellite spin and attitude precession, the error bar magnitude (resulting from the dot product of the nominal acceleration "noise" vector into the inertial "flux" axis)

will vary accordingly. The resultant error can be considered random if the nominal coordinate system varies quasi-randomly with respect to the inertial coordinate system.

The response time of the CACTUS accelerometer is slow. How much this problem can be overcome in the future is open to question. It is evident that the slow response time creates difficulties in estimating the solar transitions through the earth's terminator (see Duhumel and Marchal, 1978).

Actual calculations of the individual flux components from the accelerations in an inertial coordinate system are carried out directly and indirectly. The solar irradiance term (K↓) is deduced from solar terminator crossings. Longwave emission (L↑) can be monitored during the hightime period whereas determining reflected shortwave (K↑) requires the assumption of longwave constancy over a 24-hour period. Thus nighttime L↑ in conjunction with K↓ estimates K↑ as a residual. Analysis of Earth radiation budget components from CACTUS measurements are described by Lala et al. (1977,1978), Barlier (1978), Bouttes (1978), and Boudon et al. (1978).

## Synopsis

This section covered a wide range of material. The referenced articles provide many additional details about various instruments used to measure radiant power and their underlying physical principles. Because readers of this report are likely to be less familiar with the radiation pressure method, a more lengthy description was provided. Note that fundamentally different instrument systems (e.g., thermal vs. photon) have been used to measure radiant power for many years. Radiation pressure measuring systems add yet another dimension to our instrument array.

## 5. SENSOR IMPLEMENTATION

With the physical principles of measurement methods in mind, this section presents a discussion of the existing and potential sensor candidates to measure the radiation budget in the 1980's. First, we review the targets. Figure 5.1 shows the time variation of the Earth radiation field as would be measured by a flat-plate detector.

It is essential to consider the basic radiation budget accuracy requirements (absolute accuracy, reproducibility or precision and periodicity) as well as the special requirements of calibration and system stability and lifetime. In addition, consider the requirements imposed by various sensors on the spacecraft systems (see Section 6). We matrix the candidate sensors against these requirements in Table 5.1. A relative index is used ranging from 1 = no problem to 10 = major problem; TBD indicates to be determined.

Table 5.1 includes a convolution of many factors. It does not necessarily provide inferences regarding the conclusions of the present study. These conclusions are given in Section 9 where additional facts are considered beyond sensor potential (e.g., ability to meet sampling needs, analysis complexity, relative cost, redundancy). At this point it suffices to note the critical problems encountered by the potential sensors.

Aside from the cavity lifetime (TBD), this class of sensors suffers from a difficulty in filtering. Filter wheel movement must wait for the detector to respond. Permanent filters impair a space

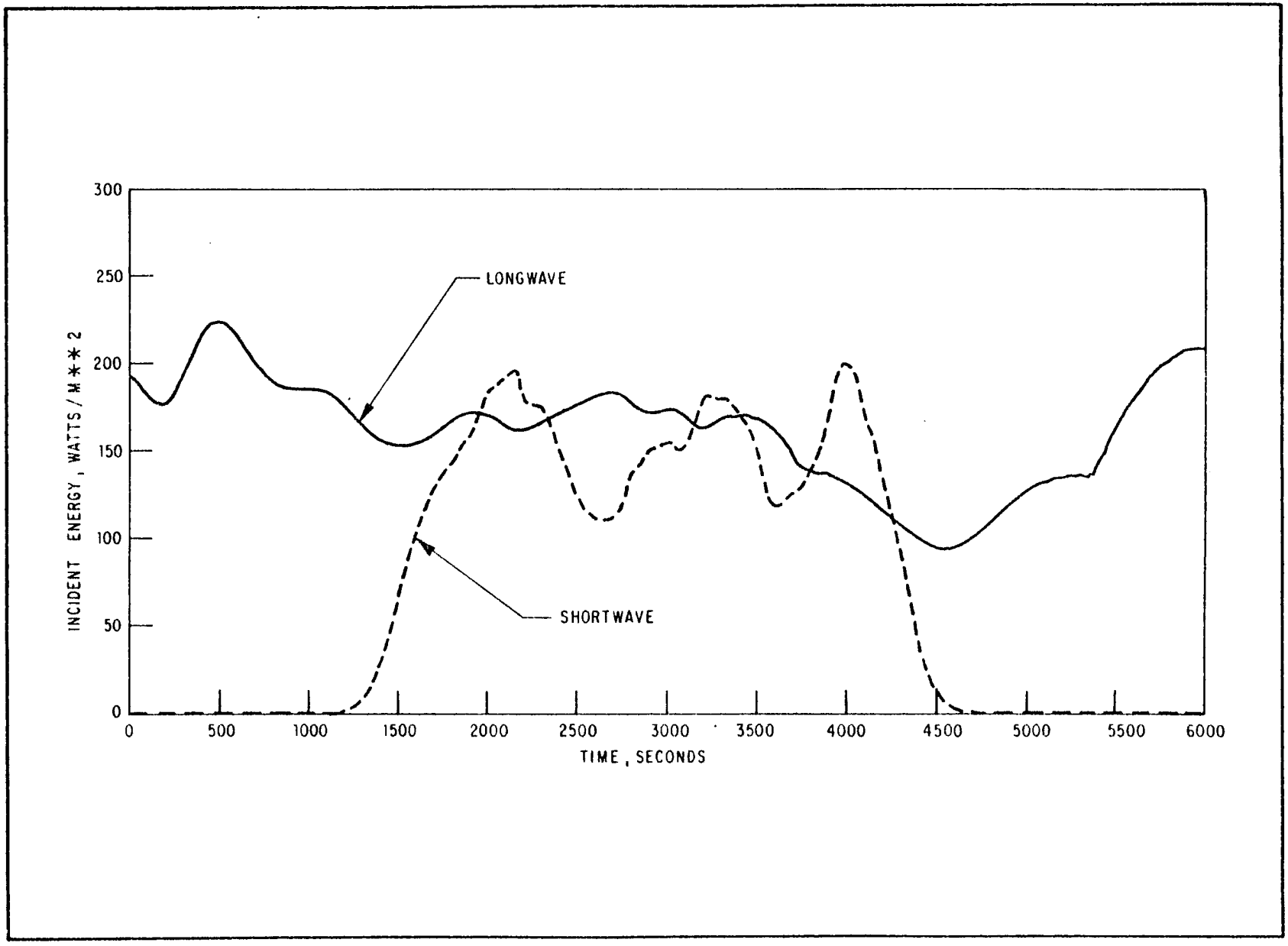


Figure 5.1. Shortwave and Longwave Radiation Incident to the Spacecraft at 833 KM (September)

Table 5.1: Sensor Relative Merit Matrix

| Req. | Cavity | WFOV Thermopile | Pyroelectric Scanner | RP Accelerometer | Photodetecto Scanner |
|---|---|---|---|---|---|
| Direct Solar | | | | | |
| Total | | | | | |
| A | 2 | 4 | 6 | 5 | 5 |
| R | 1 | 2 | 3 | 3 | 5 |
| Spectral | | | | | |
| A | 4 | 4 | 6 | 9 | 5 |
| R | 3 | 3 | 5 | 9 | 5 |
| Earth Radiation | | | | | |
| Reflected | | | | | |
| A | 5 | 4 | 7 | 5 | 7 |
| R | 4 | 2 | 4 | 4 | 5 |
| Emitted | | | | | |
| A | 5 | 3 | 2 | 4 | 8 |
| R | 4 | 2 | 1 | 3 | 8 |
| Overall R. B. | | | | | |
| Periodicity | 2 | 2 | 4 | 2 | 4 |
| Specificity | 3 | 8 | 1 | 8 | 1 |
| Calibration | | | | | |
| (Ground & Inflight) | 1 | 4 | 1-IR 6-Solar | 4 | 5 |
| Lifetime | TBD | 3 | 5 | 2 | 7 |
| Spacecraft Demands | | | | | |
| Stability | 2 | 4 | 5 | 5 | 5 |
| Thermal Control | 5 | 6 | 3 | 1 | 1 |

reference check of the cavity. Thermopiles such as the wide field-of-view (WFOV), have overall medium to good merit rank. They do suffer from thermal transients. Even though their lifetime is potentially very long, they die when the spacecraft dies.

Pyroelectric detectors are used to characterize a typical scanner system (e.g. Nimbus-7). It is difficult to calibrate the solar side of these detectors in an absolute sense, especially after launch. New methods are under study, yet past experience leaves uncertainties of ±10-15%. The scanner is definitely subject to spacecraft attitude variabilities and the sensors are sensitive to microphonics.

A radiation pressure sensor (accelerometer in small satellite with large A/M ratio) has severe difficulties determining the detailed spectral distribution of the radiation flux. This impacts spectral solar measurement as well as simple separation of Earth energy into albedo and infrared components. Spacecraft stability, arising from a variety of perturbations, due to spacecraft shape, size, and mass are other concerns. The required orbit altitudes ($\approx$ 1000 Km) excludes high resolution measurement specificity.

Sensors of the photodetector type are not well suited for measuring total emitted radiation from the Earth. Their overall accuracy and reproducability in addition to their lifetime are also in question.

Some factors of common concern among several sensors are the degradaton (by age or contamination) of surface coatings, filter optics, etc. The scanners especially suffer from these problems. The unfiltered cavities have much less of a problem. The angular response is of concern only for the WFOV thermopile (scanner analysis difficulty due to limited angular coverage is not a sensor property - See Section 7 for discussion).

Obviously, scanners use many separate measurements to assemble the large-scale radiation budget picture and thus impose greater demands on satellite data storage and transmission systems. On the other hand, WFOV and RP sensors lack the measurement specificity in space to meet certain science requirements.

It is instructive to illustrate the performance of the various solar sensors included in the above discussion. Figure 5.2 illustrates a time series of the channel 3 total solar channel on Nimbus-6. This detector responds over the bandpass 0.2-50 $\mu$m unobstructed by imaging optics filters or windows. The detector itself is a wirewound thermopile (see Jacobowitz et al., 1975). The graph consists of daily averaged percent deviations from a distance corrected solar mean value. Note with the exception of a few outliers in December, 1975, the peak to peak excursions are less than 0.2% or approximately 2.75 $W/m^2$. Although the relative accuracy (precision) of Nimbus-6 solar channels appear very good, the absolute performance indicated some problems. Discussion is given in Hicket et al., 1977.

Figure 5.3 provides initial results from the Nimbus-7 Experiment Team for the channel 10C active cavity radiometer. The first 5 months indicate excursions no larger than approximately 2 $Wm^{-2}$ (0.15%).

Figure 5.4 provides 3 years of monthly mean acceleration data from the CACTUS acceleration on board the D5B satellite. It is important to note that the variation due to earth-sun distance is easily detected. Noting that solar parameter changes on the order of 0.5% (with respect to a mean annual solar constant) will theoretically lead to significant climatic drift, the value of multiple and independent solar measurements becomes clear. It is difficult to ascertain from a single sensor

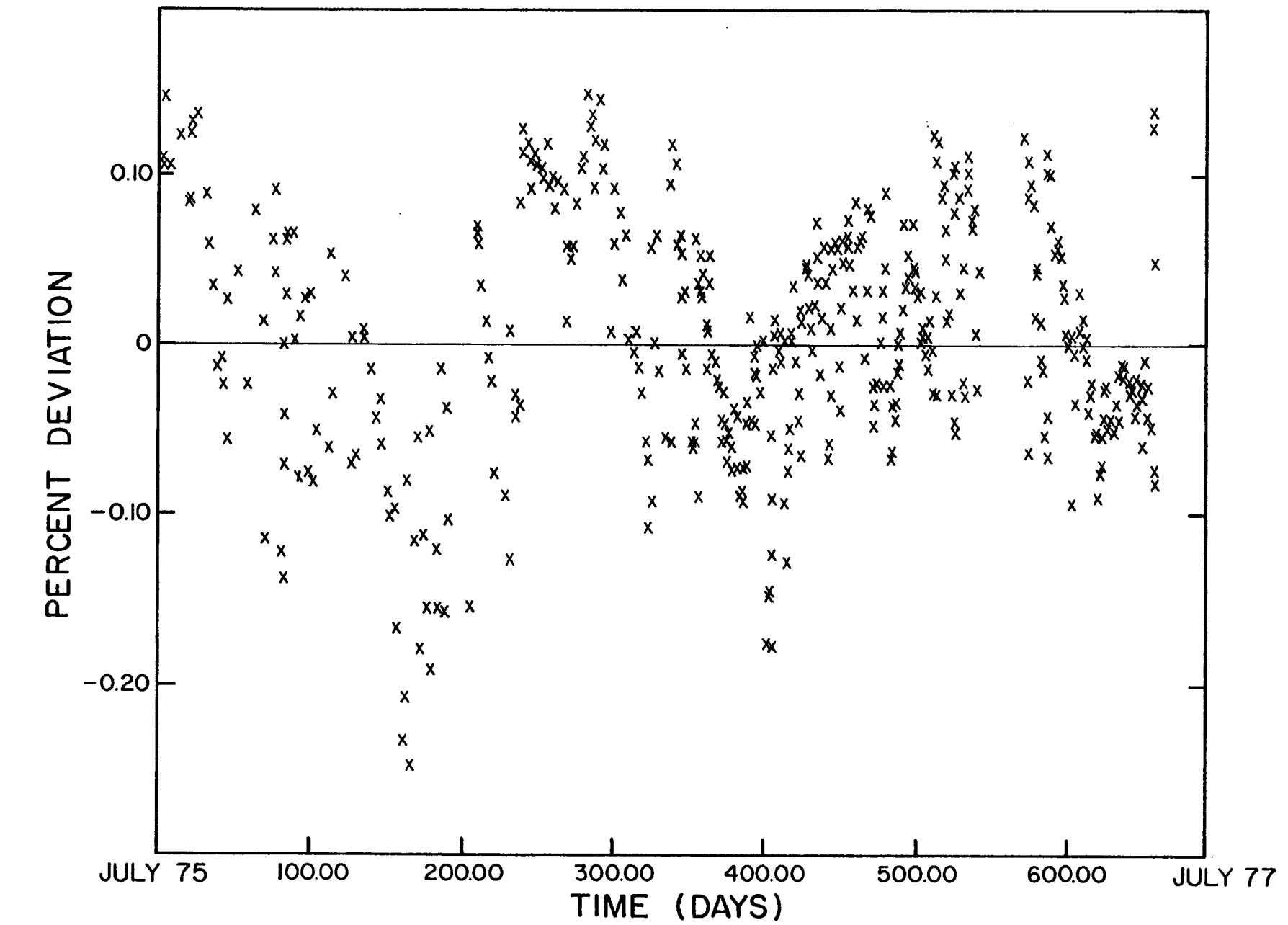
PERCENT DEVIATION FROM MEAN - SOLAR DATA (DAILY AVG.) ON CHNL 3
PERCENT DEVIATION
0.10
0
-0.10
-0.20
JULY 75
100.00
200.00
300.00
400.00
500.00
600.00
JULY 77
TIME (DAYS)

Figure 5.2

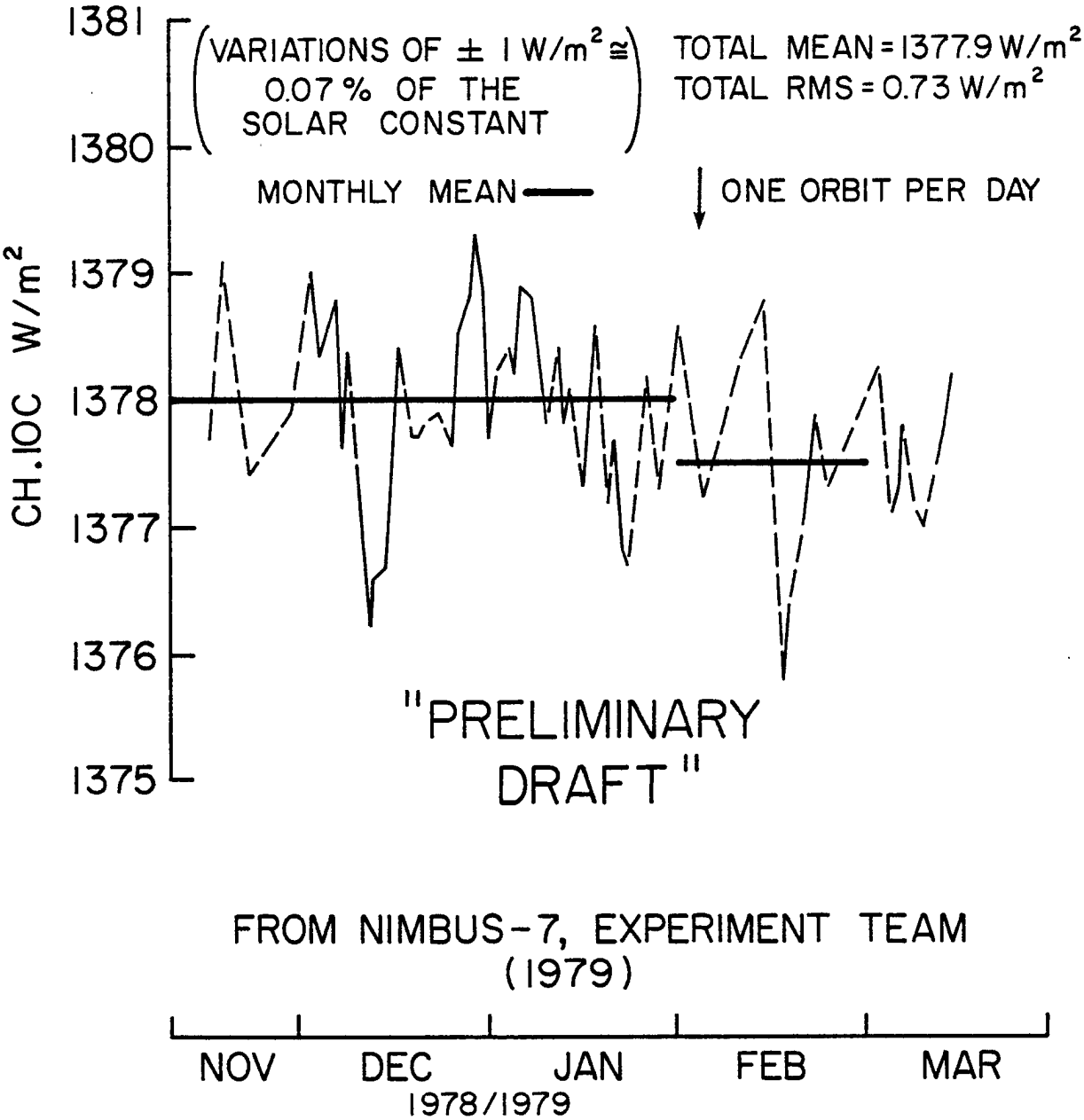


Figure 5.3: Daily Monitoring from NIMBUS-7 ERB for the Solar Constant (CH. 10C)

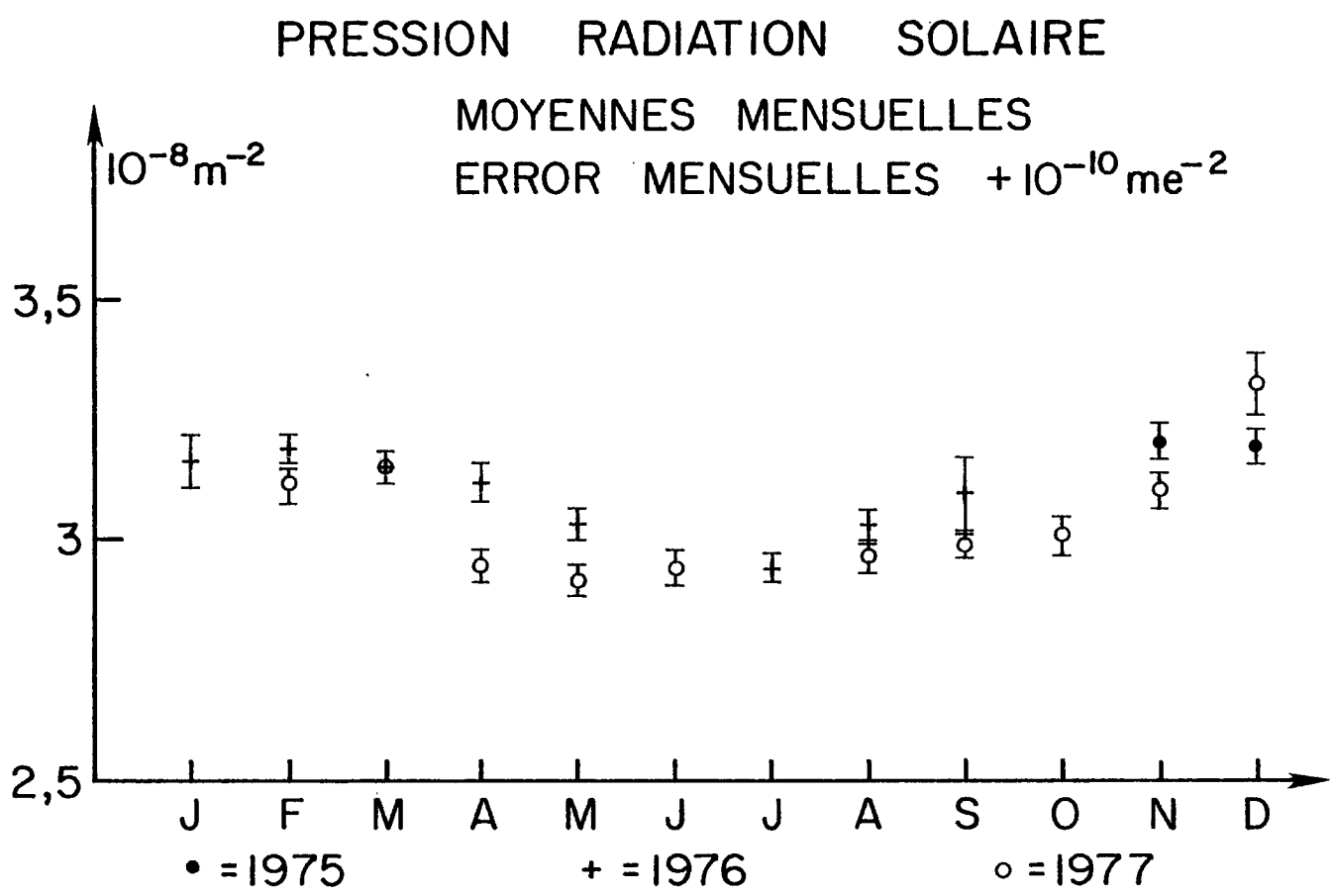
PRESSION RADIATION SOLAIRE
MOYENNES MENSUELLES
ERROR MENSUELLES +10⁻¹⁰ me⁻²
10⁻⁸m⁻²
3,5
3
2,5
J F M A M J J A S O N D
• =1975
+ =1976
o =1977

Figure 5.4

whether a 0.3-0.5% drift is instrument related or real. Confirmation by or disagreement with a second system measures the liklihood of detecting actual solar variability.

## 6. PLATFORM AND SPACE SYSTEM REQUIREMENTS

Four topics are considered as apropos to a discussion on actual inflight requirements:

1. Orbital configuration
2. Attitude determination
3. Calibration procedures.
4. Lifetime

The actual orbital configuration selected for an RP mission is affected by the same constraints as that of the 1980's ERBS program. In principle, if an exact model of the diurnal modulation of the reflected and emitted earth energy terms were known, a single polar orbiting sun synchronous satellite would accomplish the required global sampling. In fact, one of the more elusive descriptions of the earth energy budget is the diurnal modulation. As a result systems of satellites are actually required to effectively and thoroughly monitor the heat exchange process. A summary of the required orbital configuration for a single, double, triple and quadruple satellite system is given in Table 6.1 as calculated by Campbell and Vonder Haar (1978). Note there are various options when considering the first three satellite ensembles.

A second navigational consideration is the knowledge of satellite attitude. If we consider a measurement vector $\vec{P}$ in some arbitrary accelerometer frame of reference, we require the dot product of that vector with the z-axis (flux axis) considered in an inertial frame of reference. This frame of reference can only be established with a

Table 6.1: Optimal Satellite Orbits For Radiation Budget Purposes

| No. of Satellites/Orbit Configurations | | |
|---|---|---|
| 1 | or | SS<br>50-60 |
| 2 | or | 80-50<br>SS-SS |
| 3 | or<br>or | 80-80-80<br>80-60-50<br>SS-SS-50 |
| 4 | | SS-SS-80-50 |

i SS indicates sun-synchronous
Numeric indicates orbital inclination

ii Note that any configuration that is weighted heavily toward sun-synchronous observations is subject to the theoretical diural model employed to estimate 24-hour totals.

iii The first option in the 3 satellite system (80-80-80) would be an extremely difficult orbital configuration to achieve. Orbital injection maneuvers would have to be very accurate.

definition of the satellite axis with respect to the Earth. We can express the transformed flux vector ($\vec{F}$) since:

$$\cos\theta = \vec{F} \cdot \vec{P}$$

where $\theta$ is the angle subtended between the acceleration vector in the accelerometer frame of reference and the z-axis in the plane containing the two vectors.

If we express the above in differential form and dividing both sides be $\vec{F}$, we find:

$$\delta\vec{F} \cdot \vec{F}^{-1} = \left|\tan\theta\delta\theta\right| + \left|\delta\vec{P} \cdot \vec{P}^{-1}\right|$$

and

$$\% \text{ error } \vec{F} = \left|\tan\theta\delta\theta\right| + 0$$

The above assume $\vec{P}$ contains no error. Substituting the present specification value for $\delta\theta = 0.3^{\circ}$ at $\theta = 45^{\circ}$, we find that the percentage error in the flux due to attitude imprecision is on the order of 0.5%. This value is slightly higher than the accepted precision (relative) accuracy specified by COSPAR WG6 (1978). Our recommendation is to improve this specification by a factor of 2.

As noted by Crommelynek (1978) a simple, low cost satellite is highly desirable for radiation budget monitoring. The usual advantage gained by simplicity is long life; this appears to be the case with the BIRAMIS concept. Our contention is that a significantly long satellite lifetime is one of the keys to specifying the transient nature of the global energy budget. In this instance a significant lifetime is tanamount to an 11-year solar cycle. While we understand clearly the potential increase in costs,

necessary to augment the satellite with enough power capability to achieve an 11-year life span, we suggest that a continuous data set is worth the investment.

It should be noted that the relative change in heat exchange is the primary mechanism by which global climatic models are forced, not by absolute levels. A continuous data set with minimal bias variability is far more suitable to climatic studies than a data set retaining intercomparison problems. Perturbations as a result of changing instruments may well swamp any actual perturbations contained in the time series.

Some final comments are needed on the subject of instrument calibration. The calibration of a satellite detector is a process which begins long before the satellite is launched and does not terminate until the satellite or instruments eventually fail. Preflight sensitivity and gain calculations are not sufficient information as most radiometers undergo changes in their response properties after launch. It is thus customary to include as part of any instrument system, an inflight calibration procedure. Historically, this has meant viewing targets of known properties such as space, thermally controlled shutters, the sun or moon, exercising the electronics with known step functions, and/or applying the method of transfer calibrations.

As COSPAR WG6 (1978) pointed, the absolute calibration of radiometers with radiometric techniques is not the desired solution. Instead the principle of electric substitution was suggested and now is the approved approach utilized for the two Nimbus ERB experiments. In addition, the channel 10C active cavity on Nimbus-7 is constructed with a redundant hidden cavity interfaced to the same thermopile. This cavity is periodically exposed to the solar source and thus provides a check on the degradation of its mate. Limited exposure insures limited UV and proton damage

and a shared thermopile insures true equivalence. Thus, the cavity approach has dual calibration options. It is also important to note that the radiometric approach utilizes an internationally accepted radiometric scale (World Radiometric Reference, WRR), see Frohlich (1976). This scale, in turn, is referenced to pre-existing radiometric scales such as the International Pyrheliometric Scale (IPS-1956) and other radiometric references such as that used by the U.S. National Bureau of Standards.

Although the radiation pressure approach has no base scale to which to refer, it is not devoid of sophisticated calibration procedures. In fact, the accelerometer can employ a procedure analogous to that of electrical substitution, i.e., mass redistribution. In this case, known internal forces are imposed on the system thus inducing the accelerometer to respond. Deviations from the theoretical response would reflect sensitivity changes in the accelerometer itself. Since this procedure is the only independent check on accelerometer performance, it is suggested that a mass redistribution subsystem be given the highest scrutiny.

## 6.1 Notes on the Satellite Subsystems

Data recording and transmission, thermal environment and power are additional factors involved with any total measurement system. For systems such as the ERBSS, NASA (Woerner et al., 1977) has completed an extensive study of subsystem and interface requirements. ESA has done the same for SEOCS and BIRAMIS. Thus, only the following facts of special interest are included in the present report. It should be noted immediately

that bandwidth requirements for data transmission are low due to the non-spectral nature of the radiation pressure satellite. Thus, there is no need to pursue this topic.

BIRAMIS requirements include the need for no moving parts on the spacecraft. In addition, the solar cells used for power generation perturb the BIRAMIS coating, a fact that has been included in error analysis (Mainguy et al., 1979).

Solar measurements using any of the radiometers may require a special sun sensor to determine when the sun is precisely on-axis. Such devices are commonly available and may be considered part of the direct solar measurement instrumentation. Gimbals or other methods to make fine adjustments to the radiometer orientation preclude movement of the entire satellite.

Synopsis

Orbits, attitude, calibration in space and long lifetime are key earth radiation budget measurement requirements placed on satellites and their subsystems. In contrast to other missions, payload weight and data rate demands are modest.

Special efforts to determine the inflight calibration and intercomparison of the radiation budget instruments have been a part of all conceptual studies. In addition, the concept of a system of satellites to measure radiation budget, thus attacking the time and space sampling problem, has required use of new and complex simulation studies. Work is continuing in all these areas for mid-1980 experiments.

## 7. DATA ANALYSIS REQUIREMENTS

Although radiometric measurements and radiation pressure measurements involve different detection principles and calibration methodology, both involve similar analysis procedures. For the sake of simplicity, the analysis of calibrated raw measurements (the response characteristics of the detector or radiation receiver are assumed to be known at this point) falls into four broad categories:

a. Navigational correction

b. Flux deconvolution

c. Statistical averages

d. Post hoc verification

### a. Navigational Correction

Presumably the orbital characteristics of any satellite are known well enough to eliminate the possibility of satellite mislocation errors. Nominal accuracies provided by range, range-rate tracking techniques provide orbital fixes on the order of 30 arc seconds during the course of an orbital period. This translates to a location error of 0.15 km for a 1000 km satellite orbit, which is considered insignificant for budget purposes. Satellite attitude on the other hand represents a potential first order error source for either type of satellite system. Let us consider three types of satellite attitude characteristics: 1) fixed with respect to a celestial reference; 2) stably precessing with respect to a celestial reference; 3) irregular orientation with respect to a celestial reference.

Type 1 and 2 systems are far more desirable than type 3 systems in that the latter case requires accurate on-board attitude sensors. The first two cases may or may not involve on-board attitude sensors. This is because if the characteristics of the attitude are well defined, the orientation vector can be solved for as a function of time from the data base itself. Ideally, the satellite attitude would be relatively stable and the satellite itself would carry on-board attitude sensing detectors.

There are two troublesome aspects of varying attitude containing a random error term. Assume the attitude vector is described by

$$\vec{A}(t) = \vec{A}_o(t) + \vec{A}_r(t) \qquad (7.1)$$

where $\vec{A}_o(t)$ represents the mean precessing attitude vector and $\vec{A}_r(t)$ represents an unknown random component. The latter component translates to errors in the angular response function applied to a radiometric instrument. In the case of an accelerometer on a radiation pressure satellite, this unknown leads to errors in the rotation from the nominal (measurement) reference frame to the inertial (flux) reference frame. Angular conditions that apply to orbital accuracy no longer apply to attitude accuracy except at the sub-satellite point. Assuming that the radiative source region needs to be specified to an accuracy of 1 km the $\vec{A}_r(t)$ component must be no greater than 2 arc minutes for a 1000 km satellite. In considering the $\vec{A}_o(t)$ component, it must be realized that if the time variability is large and not periodic (thus requiring occasional discontinuous attitude maneuvers), a terrestrial radiative source region will vary according to a fixed satellite position since the earth cannot be considered as a point source. This problem can be somewhat overcome during a deconvolution, but with respect to an ideal system,

presents an aggravating variability term. In the case of a radiation pressure system, if the $\vec{A}_o(t)$ component is fixed or slowly precessing according to known characteristics, it can be solved for by utilizing a pair of transit time measurements (day/night, night/day) and assuming constancy of the solar source over a half orbital period. This is somewhat advantageous over a radiometric system such as the ERB instrument, in which mechanical maneuvering is required for repeated views of the sun. Of course, if the maneuvering characteristics and their effect on the satellite are known perfectly, the same principles would apply to a radiometric system. This is generally not the case.

b. Flux Deconvolution

The difficulty with wide field-of-view measurements, with respect to earth fluxes (measurements which characterize both WFOV radiometric and radiation pressure measurements) is the transformation of satellite altitude fluxes to normalized constant altitude fluxes, preferably at an altitude synonymous with the top of the atmosphere; see Figure 7.1 from Houghton (1979) for an explanation. This is an essential process in case of an eccentric orbit or in making comparisons to other measurements. Although it would be possible to monitor radiative modulation of the earth system at an arbitrary constant altitude reference, it would be difficult to apply such measurements to climate or general circulation models which are presently designed according to specific zonal structures. Furthermore, it would be nearly impossible to develop a useful historical record, involving various satellites and satellite systems, without normalizing to a constant reference level, i.e., the top of the atmosphere. The following discussion outlines an analytically based deconvolution model which would be used to transform radiative fluxes from the satellite altitude surface to the top of the atmosphere surface.

Figure 7.1

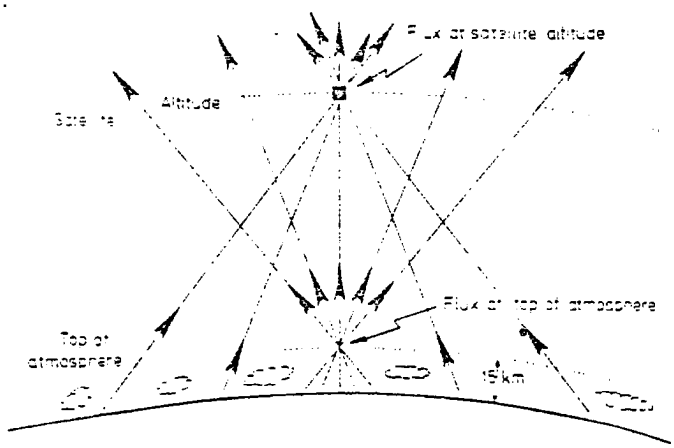


Illustrating the problem of relating the outgoing radiative flux at the top of the atmosphere to measurements at a typical satellite altitude.

A relationship exists between top of atmosphere fluxes and satellite altitude fluxes if certain assumptions are satisfied. Essentially the two dimensional integral equation relating sources to measurement can be inverted, provided that the average emission or reflection characteristics depend only on the relative position of the source flux and measurement sensor. This assumption is adequately satisfied for infrared flux with respect to a time average. It is not adequate for reflected flux since the strong bidirectional reflectance characteristics of the earth are correlated with variation in surface and atmospheric reflecting features. With respect to zonal averages, this difficulty can be overcome by the application of an angular reflectance model.

A flux $m(\theta_s,\phi_s,t)$ is determined at the satellite wrt location $(\theta_s,\phi_s)$ at time $t$. This measurement can be expressed in terms of a flux $s(\theta_a,\phi_a,t)$ at the top of the atmosphere wrt location $(\theta_a,\phi_a)$ and a weighting function $g(\theta_a,\phi_a,\theta_s,\phi_s,t)$:

$$m(\theta_s,\phi_s,t) = \int s(\theta_a,\phi_a,t)g(\theta_a,\phi_a,\theta_s,\phi_s,t)\frac{d\Omega}{\pi} \qquad (7.2)$$

The weighting function can be considered as a multiple of two terms: a detector angular response function $h(\gamma)$, which depends on the relative positions of $(\theta_a,\phi_a)$ and $\theta_s,\phi_s)$; and an anisotropic bidirectional normalization factor $\chi(\theta_a,\phi_a,\theta_s,\phi_s,t)$, which involves the dependence on absolute position:

$$m(\theta_s,\phi_s t) = \int s(\theta_a,\phi_a,t)\ (\theta_a,\phi_a,\theta_s,\phi_s,t)h(\gamma)\frac{d\Omega}{\pi} \qquad (7.3)$$

where:

$$\gamma = \cos^{-1}(\vec{r}_e \cdot \vec{r}_s), \tag{7.4}$$

$\vec{r}_e$ = source vector

$\vec{r}_s$ = satellite vector

Clearly a time average is needed to obtain a reasonable measure

$\bar{m}(\theta_s,\phi_s)$ where:

$$\bar{m}(\theta_s,\phi_s) = \frac{\int m dt}{\int dt} = \int \frac{\int s\chi dt}{\int dt} \; h \; \frac{d\Omega}{\pi} = \int \frac{}{sp} \; h \; \frac{d\Omega}{\pi} \tag{7.5}$$

Now let us assume that in the average, the source flux is not correlated with the varying part of $\chi(t) = \chi_o(t) + \chi(t)$ where $\chi_o(t)$ is nearly constant close to one. Thus:

$$\int \overline{s\chi} dt = \chi_o \int \bar{s} dt \tag{7.6}$$

and therefore substituting:

$$\bar{m}(\theta_s,\phi_s) = \chi_o \int \bar{s}(\theta_a,\phi_a) h(\gamma) \frac{d\Omega}{\pi} \tag{7.7}$$

This integral equation can be inverted since spherical harmonics are eigen-functions of the operator $\int h(\gamma) d\Omega$.

Expanding $\bar{m}$, h, and $\bar{s}$ in spherical harmonics:

$$\bar{m}(\theta_s,\phi_s) = \sum_{n=0}^{\infty} \sum_{\ell=-n}^{n} m_n^{\ell}\, Y_n^{\ell}(\theta_s,\phi_s)$$

$$h(\gamma) = \sum_{i=0}^{\infty} h_i\, P_i(\cos\gamma) \qquad (7.8)$$

$$\bar{s}(\theta_\alpha,\phi_\alpha) = \sum_{j=0}^{\infty} \sum_{k=-j}^{j} s_j^k\, Y_j^k(\theta_\alpha,\phi_\alpha)$$

Where P's are Legendre polynomials and Y's are spherical harmonics.

Thus $\bar{m}(\theta_s,\phi_s)$ is defined:

$$\bar{m}(\theta_s,\phi_s) = \lambda_o \sum_{j=0}^{\infty} \sum_{k=-j}^{j} \sum_{i=0}^{\infty} \int h_i\, s_j^k\, Y_j^k(\theta_\alpha,\phi_\alpha)\, P_i(\cos\gamma)\, \frac{d\Omega}{\pi} \qquad (7.9)$$

Using the addition theorem for spherical harmonics (See Arfken, 1970):

$$P_i(\cos\gamma) = \left(\frac{4\pi}{2i+1}\right) \sum_{q=-i}^{i} Y_i^q(\theta_s,\phi_s)\, Y_i^{q*}(\theta_\alpha,\phi_\alpha) \qquad (7.10)$$

Thus the measurement becomes:

$$\bar{m}(\theta_s,\phi_s) = \lambda_o \sum_{j=0}^{\infty} \sum_{k=-j}^{j} \sum_{i=0}^{\infty} \sum_{q=-i}^{i} h_i s_j^k\, Y_i^q(\theta_s,\phi_s) \qquad (7.11)$$

$$\cdot \left(\frac{4\pi}{2i+1}\right) \int Y_j^k(\theta_\alpha,\phi_\alpha) Y_i^{q*}(\theta_\alpha,\phi_\alpha)\, \frac{d\Omega}{\pi}$$

Since spherical harmonics are an orthonormal set:

$$\bar{m}(\theta_s,\phi_s)=\chi_o \sum_{j=0}^{\infty} \sum_{K=-j}^{j} \sum_{i=0}^{\infty} \sum_{q=-i}^{i} n_i s_j^K Y_i^q(\theta_s,\phi_s)\cdot\left(\frac{4\pi}{2i+1}\right)\cdot \delta_{ij}\cdot\frac{1}{\pi} \qquad (7.12)$$

where $\delta_{ij}$ is the Dirac delta function. By simplification:

$$\bar{m}(\theta_s,\phi_s)=\chi_o \sum_{j=0}^{\infty} \sum_{K=-j}^{j} h_j s_j^K Y_j^K(\theta_s,\phi_s)\left(\frac{4}{2j+1}\right) \qquad (7.13)$$

Comparing the series expansion of $\bar{m}(\theta_s,\phi_s)$, the corresponding coefficients can be found:

$$\sum_{j=0}^{\infty} \sum_{k=-j}^{j} m_j^k Y_j^k(\theta_s,\phi_s) = \chi_o \sum_{j=0}^{\infty} \sum_{k=-j}^{j} h_j s_j^k Y_j^k(\theta_s,\phi_s)\left(\frac{4}{2j+1}\right) \qquad (7.14)$$

Finally:

$$s_j^k = \frac{2j+1}{4}\cdot\frac{m_j^k}{h_j}\cdot\frac{1}{\chi_o} \qquad (7.15)$$

Thus, a reasonably accurate measurement of $\bar{m}(\theta_s,\phi_s)$ will determine the source function $\bar{s}(\theta_a,\phi_a)$ if $h(\lambda)$ and $\chi_o(t)$ are known.

c) Statistical Averages

The process of creating terrestrial radiative averages needs one word of caution. In the deconvolution, it was noted that for a given time constant, the average emission and reflection characteristics need to be described in order to properly invert the integral equation relating nominal measurements to atmospheric fluxes. A time constant ($\Delta t_{bd}$) associated with the angular model applied to the deconvolution,

represents a limiting averaging time. In conjunction with this time constant, is a sampling distribution of measurements for given zones. Ideally, this distribution would be flat; if not, the signal to noise characteristics of individual zones would vary. Thus, a second time constant ($\Delta t_{sn}$) may need to be imposed to reduce the maximum n/s ratio to a "not to exceed" specification. The selection of optimal orbits as discussed in Section 6 minimizes the later problem.

d) Post hoc Verification

Exact verification of a set of independent radiation measurement after the analysis has considered all of the physical and numerical steps needed to generate energetic units, would require a second set of independent measurements considered to be an exact reference. Of course, this is not now possible from remote platforms, although future space shuttle missions present an opportunity to independently verify radiation budget missions. On the other hand, two independent sets of measurements using fundamentally different detection principles, provide a much more powerful data base than any single set. To these authors, one of the most valuable aspects of a radiation pressure satellite, would be its ability to monitor the radiative output of the sun as an independent check on modern satellite cavity radiometers. Indications of perturbations and/or anomalous solar activity cannot be completely trusted when considering a single instrument. Two independent measurements of the same phenomona utilizing different measurement principles reduces the probability for error dramatically.

Synopsis

In recent years the impact of assumptions and necessary approximations during data analysis has been recognized as a potential major contributor to overall uncertainty in satellite experiment results. For this reason the foregoing discussion has been presented in a general sense, applicable to all satellite experiments under study. We have not discussed here a powerful tool to explore the impact of analysis, namely the computer simulation of a space experiment. Methods used to "fly the satellite in the computer" prior to satellite launch should be the subject of further study.

## 8. POSSIBLE COMPLEMENTARY SYSTEMS

The appeal of the BIRAMIS concept stems from its inherent simplicity, an important factor for longterm climate applications. This requirement has been specifically addressed by COSPAR Working Group 6 in their report on "Observing Systems for Radiation Budget Studies". In addition, by use of alternate physical principles than conventional radiometry, with attendant differences in engineering, it offers an alternate or "second way" to measure the radiation budget. All high accuracy and precision space measurements, especially at the beginning of the climate program, will fall under heavy scrutiny by scientists. For this reason alone, availability of alternate concepts must be explored. A complementary measurement program would thus involve sensors of both the radiometric and radiation pressure types. Such a system could simply be a mix of the separate experiments flying at the same time.

Thus, further study should be directed toward a composite sensors, one that simultaneously measures the radiation budget (perhaps only the direct solar energy as a start[1]) by employing both principles. We believe the BIRAMIS design concept, in conjunction with a small cavity similar to the IOC channel on Nimbus-7, provides a composite sensor independently measuring both radiation pressure and radiation flux. Since the A/M ratio would be high, the active elements of the radiometer could be inside the sphere. The most attractive aspect of such a composite concept is the possibility to determine, from the two separate

---

[1] Prag, personal communication (1979)

measurements, both the desired incident radiation and the absorptance of the sphere's coating. As was shown in Section 4, varying absorptance properties introduces uncertainty in both methods when deployed independently, and requires extra inflight calibration procedures. Assuming, for example, that the black honeycomb coating is the common surface for both measurements, a composite sensor system would eliminate the major concern about absorptance change.

The composite concept can also be considered for a direct measurement of global net radiation. The global average power reflected and emitted through a surface at satellite altitude measured radiometrically by a plate is equivalent in principle to that measured by a spherical radiation pressure receiver utilizing a tri-axial accelerometer. Sampling requirements (See Section 6) would be the same as for other systems. Values of net radiation from such a composite system, flying in orbits near 1000 Km, would provide regional and radiation gradient information of use for climate purposes. Its interpretation at these scales would require special treatment as shown in Section 7 and Campbell and Vonder Haar (1978).

Direct solar energy measurements from a radiation pressure satellite are determined from low orbits by using terminator crossing data following Suomi et al. (1967). On a composite system additional approaches are possible since the two separate measurements could be designed to have different time constants, etc., thus providing improved means to separate Earth radiation from direct solar radiation.

Finally, since direct solar measurements are so important to the climate program, the composite method satellites could be deployed into far Earth orbits or simply sent out of Earth orbit at periodic intervals.

Synopsis

Work during the course of the present study has led us to propose to ESA that a BIRAMIS with the black honeycomb coating carry several small cavity radiometers. These few "active" honeycomb cells would allow the complementary measurement of radiation budget and/or direct solar output by the two different physical principles from the same satellite.

## 9. APPLICABILITY OF THREE RADIATION BUDGET MEASUREMENT METHODS

Previous studies such as that by COSPAR Working Group 6 (1978) have provided general surveys of various approaches to the radiation budget measurement problem. The present work is more detailed and culminates in the following conclusions concerning the applicability of (a) the radiometric method (b) the radiation pressure method and (c) the composite method to the primary radiation budget requirements.

### A. Conclusions About Physical Principles and Basic Concepts

1. Both modern radiometry and the radiation pressure concept are based on independent but sound physical principles.

2. Analysis of the D5B-CACTUS data demonstrated the existence of the radiation budget components in the acceleration data. It is important to note that this system was not designed for an earth radiation budget experiment, but was an atmospheric density experiment. It demonstrated proof of concept for the radiation pressure method.

3. Analysis has shown that accelerations due to various parasitic forces can be overcome for the radiation pressure method. The development of a surface coating (either polished aluminum or black honeycomb light traps) with the required radiative properties does not appear to represent a major problem.

4. Because of the variable angular distribution of terrestrial radiation, accurate knowledge of the accelerometer orientation (spacecraft attitude) is required so as to properly transform to a flux representation. The same is true for a flat plate radiometer system, although for a different reason. In this case, the response function of

the receiver (cosine response characteristics) dictates knowledge of the receiver plate orientation with respect to the radiative source.

5. The sensitivity of the RP system is controlled by the A/M ratio. The area factor (A) is limited in terms of a given launch vehicle. The limitation may be relaxed if a space shuttle launch is considered.

6. The sensitivity of the radiometric system depends primarily on isolation from transient thermal and radiation fields arising for the satellite and field stops.

B. Conclusions About Error Limits

1. The present cavity radiometer on Nimbus-7 has demonstrated high absolute and high relative accuracy.

2. The present BIRAMIS Payload Study (Onera, 1979) indicates measurement error levels which are marginal for absolute solar monitoring when considered by themselves. Earth component accuracy is satisfactroy in terms of existing accuracy requirements assuming no problems with the accelerometer sensitivity and precise knowledge of satellite attitude.

3. The direct net radiation measurements provided by a radiation pressure detector may be more accurate in a relative sense than derived net radiation measurements provided by separate radiometers.

4. The response times of modern radiometers are high. The active cavity and the WFOV thermopile channels on Nimbus-7 respond on the order of 1 second. Pyroelectric detectors respond on the order of $10^2$ nanoseconds.

5. The response time of accelerometers appears to be low ($\simeq$ 20 seconds). This may lead to problems in isolating the direct solar term at terminator excursions.

C. Conclusions About Sensor Implementation

1. The radiation pressure satellite is a relatively simple and long life system.

2. Some radiometers have a shorter lifetime because of moving parts and optics; others have long lifetimes.

3. Unlike the radiometer method, the RP method provides no simple method for spectral separation of the net radiation budget.

D. Conclusions About Platform and Space System Requirements

1. Regardless of the detection technique, multiple satellite systems are required for radiation budget monitoring to solve sampling problems.

2. Knowledge of the attitude of either satellite system is required. We suggest that the RP attitude accuracy specification of $0.3^{o}$ be improved by a factor of two or the order of $0.15^{o}$. This would yield a flux transformation error of no more than 0.26%.

3. We suggest that because of the simplicity in design of the RP system and thus the probability for a long life mission, that power considerations be considered which would extend the lifetime for a single mission to an 11-year period (complete solar cycle).

4. Although the RP method lacks an accepted calibration standard, it can utilize an analog to the electric substitution principles employed by a thermopile system, i.e., substitution of known mass redistribution forces on the accelerometer ball.

E. Conclusions About Data Analysis Requirements

1. Both satellite techniques require precise knowledge of the attitude/orbit configuration for navigational treatment of the data.

2. Estimates of top of atmospheric fluxes (e.g., deconvolution) and space-time averaging are problems common to either measurement technique.

F. Conclusions About the Composite Approach

1. The nature of the honeycomb coating design for the RP method provides a means to develop a composite system (radiometer-radiation pressure) in which one or more of the honeycomb elements is replaced by a cavity utilizing a similar black surface coating.

2. A composite approach not only offers redundant measurements but a means to solve for two independent properties, i.e., net radiation and coating absorptance changes.

3. The redundancy of the composite system suggests the option of far earth orbits for precise solar constant monitoring.

Aside from details discussin in earlier sections, the relative comparison of the three methods points out the following areas in need of further study:

1. The limiting accuracy and response time of an accelerometer.

2. The accuracy and reliability of pyroelectric cavities.

3. A computer simulation of the determination of the earth radiation budget via the radiation pressure technique utilizing realistic terrestrial radiation budget data.

Synopsis

This intercomparison study to the two basic methods to measure the earth's radiation budget, the radiometric and the radiation pressure approaches, has led to the suggestion that a third, composite approach

be given detailed study aswell. We conclude that climate requirements for net radiation budget data (a) can be met today by a system of radiometric sensors on satellites, (b) can most probably also be met by a system of radiation pressure detectors, and (c) may be met most credibly by a composite system using both principles to independently measure the same signals from sun and earth.

Because the radiation pressure method is generally less familiar to scientists at this time, we devoted more attention to it in the present study. A review of the conceptual and definition studies completed for ESA together with a review of the proof of concept results from the D5B satellite demonstrated to our satisfaction the viability of this approach as applied to certain radiation budget requirements of the climate study programs.

Of course, additional study is needed on certain aspects of all three methods and these needs are noted in earlier sections. Furthermore, it is highly advisable to subject each of the three methods to a complex computer simulation of earth radiation budget measurement. This should be done after early sensor and spacecraft studies are completed, but before instrument development begins. The procedure has been carried out the ERBSS with excellent results.

REFERENCES

Abbott, T. M. and J. C. Reed, 1974: Visible Infrared Spin-Scan Radiometer (VISSR) for a Synchronous Meteorological Spacecraft (SMS). Final Report, Contract No. NAS 5-21139, Santa Barbara Research Center, Goleta, CA.

Arfken, G., 1970: Mathematical Methods for Physicists, Second Edition. Academic Press, New York/San Francisco/London, 815 pp.

Barlier, F., 1978: Compte Rendu des Resultats Scientifiques Obtenus Avec L'accéléromètre CACTUS Embarqué a Bord du Satellite CASTOR. Groupe de Recherches de Geodesie Sputiuk, GRGS NT/68/GRASSE, 15 pp.

Barlier, F., C. Pastre, A. M. Mainguy, R. Juillerat, A. Paillous, M. Romero, J. J. Walch, Y. Boudon, and A. Cazen, 1978: Study of Atmospheric Thermal Balance by Measurement of Radiation Pressure. ESA Journal, 2 pp. 27-36.

Bernard, A., M. Gay, A. M. Mainguy, R. Juillerat, J. J. Walch, Y. Boudon, F. Barlier, and P. Lála, 1977: Radiation Pressures Determination with the CACTUS Accelerometer. Presented at the 20th Reunion of COSPAR, Tel-Aviv, 7-18 June, 6 pp.

Boudon, Y., F. Barlier, A. Bernard, R. Juillerat, A. M. Mainguy, and J. J. Walch, 1978: Synthèse des Résultants en Vol de L'Accéleromètre CACTUS Pour des Accélerations Inferieures A $10^{-9}$G. Centre d'Etudes et de Recherches Géodynamiques et Astronomiques (CERGA), Strasbourg Observatoire, France, 13 pp.

Bouttles, J., R. Juillerat, and A. M. Mainguy, 1978: Utilisation de L'accélérometrè CACTUS Pour la Mesure du Bilan Radiatif de la Terre. Extrait de la Recherche Aérospatiale n° 1978-2, Office National D'etudes et de Recherches Aerospatiales, Chatillon, France, pp. 95-97.

Brusa, R. W., E. J. Gillham, and D. Crommelynck, 1977: SEOCS Sun-Earth Observatory and Climatology Satellite - Instrument Definition - Absolute Radiometers. European Space Agency Report DP/PS(77)24, Paris, France, 45 pp.

Campbell, G. G. and T. H. Vonder Haar, 1978: Optimum Satellite Orbits for Accurate Measurement of the Earth's Radiation Budget, Summary. Atmospheric Science Paper No. 289, Department of Atmospheric Science, Colorado State University, Fort Collins, CO, 61 pp.

Chandrasekhar, S., 1960: Radiative Transfer. Dover Publications, Inc., New York, 393 pp.

COSPAR Working Gruop 6, 1978: Toward an Internationally Coordinated Earth Radiation Budget Satellite Observing System: Scientific Uses and Systems Considerations. Report to ICSU and to JOC for GARP, Results of Specialists Meeting on Satellite Observing Systems for Radiation Budget Studies, May, 1978, Alpbach, Austria - Printed by the National Center of Atmospheric Research (NCAR), 76 pp.

Coulson, K. L., 1975: Solar and Terrestrial Radiaton - Methods and Measurements. Academic Press, New York/San Francisco/London, 322 pp.

Crommelynck, D., 1978: Utilisation D'un Accelerometre Super Cactus Monte Sur un Satellite Pour L'observation "Directe" du Bilan Radiatif. Proceedings of the European Workshop on Space Oceanography, Navigation and Geodynamics (SONG), Schloss Elman, Germany, 16-21 January, p. 271-273.

Duhamel, T. and P. Marchal, 1978: Earth Radiation Budget: Simulation of Fluxes and Accelerometric Measurements. Presented at the 29th Congres International d'Astronautique - Section Etudiants, Dubrovnik, Yugoslavia, 1-8 October, 15 pp.

ESA, 1978: Sun-Earth Observatory and Climatology Satellite - SEOCS - Report on the Phase A Study. European Space Agency Report DP/PS (78)10, Paris, France, 58 pp.

Frohlich, C., 1976: Results - Fourth International Pyrheliometer Comparisons: Third Regional Pyrheliometer Comparisons (RA VI) 6-24 October, 1975, Davos, Switzerland. Working Report No. 58, Swiss Meteorological Institute, Zurich, Switzerland.

Girard, A., 1978: Influence des Propriétés Optiques du Revetement D'une Sphère Sur Lu Pression de Radiation. Rech. Aérosp - nº 1978-4, Muître de Recherche à l'O. N.E.R.A., pp. 209-212.

Handbook of Chemistry and Physics, 53rd edition, 1962: Chemical Rubber Publishing Co., Cleveland, OH.

Hickey, J. R., F. J. Griffin, and H. B. Howell, 1977: Two Years of Solar Measurements from the Nimbus-6 Satellite. Proceedings of the International Solar Energy Society Solar World Conference, June 6-9, Orlando, FL, 5 pp.

Hoffman, J. W., 1978: SEOCS Sun-Earth Observatory and Climatology Satellite - Phase A Study Final Report - Scanning Radiometer Feasibility. European Space Agency Contract Report, ESTEC Contract No. 3195/77/NL/PP(SC), Dornier System, Friedrichshafen, Germany, 46 pp.

Houghton, J. T., 1979: The Future Role of Observations from Meteorological Satellites. QJRMS, 105, 443, pp. 1-23.

Hudson, R. D., 1969: Infrared System Engineering. John Wiley and Sons, New York/London/Sydney/Toronto, 642 pp.

Jacobowitz, H., L. L. Stowe, and J. R. Hickey, 1978: The Earth Radiation Budget (ERB) Experiment. The Nimbus-7 User's Guide, Goddard Space Flight Center, Greenbelt, MD, pp. 33-69.

Lála, P., F. Barlier and G. Oyharcabal, 1978: Interpretation of the D5B Satellite Measurements and the New Model of the Earth's Albedo. Bull. Astron. Inst. Czechosl., 29/4, 238-243.

Levadon, F., 1978: Détermination de Coefficient de Poussée du au Rayonnement sur Une Sphère - Comparison de Deux Types de Revêtements Pour le Projet BIRAMIS. Draft Report, ESTEC, Nourwijk, Netherlands.

Langley Research Center, 1975: Execution Phase Project Plan for Long-term Zone - Earth Energy Budget Experiment (LZEEBE). NASA-LRC, Hampton, VA, 160 pp.

Mainguy, A. M., 1978: Evaluation of the Disturbing Accelerations and Comparison With the Accelerations Due to the Radiation Pressure. Draft Report, 12 pp.

Mainguy, A. M., A. Bernard, M. Romero, F. Barlier, and J. Bouttes, 1979: Direct Measurement of the Earth Radiation Budget by Means of an Accelerometer. Presented at the IEEE Region V Annual Conference, April 3-5, El Paso, TE, 14 pp.

Mainguy, A. M., J. Bouttes, R. Juillerat, and F. Barlier, 1978: Mesure du Bilan Radiatif de la Terre a l'aide d'un Accelerometer Ultrasensible - Projet BIRAMIS.

Onera, 1978: Proposal to ESA - Experiment for Space Qualifications of a Super-Cactus Accelerometer. ONERA, Chatillon, France, 3 pp.

Onera, 1979: BIRAMIS Payload Study. Preliminary Edition of Final Report, Contract No. 3454/77/NL/PP(SC).

Pastre, C. and Julliet, 1977: Discussion of the Principle of an Instrument to Measure Radiation Intensity by Observing Radiation Pressure (CACTUS Experiment). Draft Report.

Peckham, G. E., 1977: SEOCS Sun-Earth Observatory and Climatology Satellite-Instrument Definition - Scanning Radiometer. European Space Agency Report DP/PS(77)23, Paris, France, 15 pp.

Raschke, E., 1978: Terminology and Units of Radiation Quantities and Measurements. Report by the International Association of Meteorology and Atmospheric Physics (AMAP) Radiation Commission, Printed by the National Center of Atmospheric Research (NCAR), Boulder, CO, 17 pp.

Raschke, E., T. H. Vonder Haar, W. R. Bandeen, and M. Pasternak, 1973: The Annual Radiation Balance of the Earth - Atmospheric System During 1969-1970 From Nimbus-3 Measurements. J. Atmos. Sci., 30/3, 341-364.

Schniewind, J., 1978: On the SEOCS Sampling Problem. Internal ESTEC Working Paper No. 1118, ESA-ESTEC, Noordwijk, Netherlands.

Schniewind, J., 1978: On the SEOCS Sampling Problem - Further Results. Internal Working Paper No. 1138, ESA-ESTEC, Noordwijk, Netherlands.

Simon, P. C., 1977: SEOCS Sun-Earth Observatory and Climatology Satellite - Instrument Definition - Solar Flux Spectrometer. European Space Agency Report DP/PS(77)22, Paris, France, 25 pp.

Smith, W. L., D. T. Hilleary, H. Jacobowitz, H. B. Howell, J. R. Hickey, and A. J. Drummond, 1975: The Earth Radiation Budget Experiment. The Nimbus-6 User's Guide, Goddard Space Flight Center, Greenbelt, MD, pp. 109-139.

Smith, W. L., W. C. Shen and H. B. Howell, 1977: A Radiative Heating Model Derived from the GATE MSR Experiment. J. Appl. Meteor. 16/4, 384-392.

Suomi, V. E., K. J. Hanson, and T. H. Vonder Haar, 1967: The Theoretical Basis for Low-resolution Radiometer Measurements from a Satellite. Studies in Atmospheric Energetics Based on Aerospace Probings, Annual Report on WBG-27, Department of Meteorology, Univeristy of Wisconsin, Maddison, WI, pp. 79-100.

Tessier, R., 1977:- ESA Activities in Connection with Radiation Balance Measurements. Letter to Morris Tepper. 4 pp.

Van de Hulst, H. C., 1957: Light Scattering by Small Particles, John Wiley and Sons, Inc., London, 470 pp.

Vonder Haar, T. H. and W. H. Wallschlaeger, 1978: Design Definition Study of the Earth Radiation Budget Satellite System. Department of Atmospheric Science Technical Report CR-158934, Final Report Contract No. NAS 1-14538, Colorado State University, Fort Collins, CO.

Woener, C. V. and J. E. Cooper, 1977: Earth Radiation Budget Satellite System Studies. NASA Technical Memorandum NASA TM X-72776, Langley Research Center, Hampton, VA, 56 pp.

APPENDIX A

## INSTRUMENT ACCURACY AND PRECISION REQUIREMENTS (U.S. PROGRAM)

Instrument system end-to-end accuracy and precision requirements and goals are given in Table A.I. The following definitions are used in stating the instrument performance requirements:

### Systematic Error

The non-random uncertainty of a measurement with reference to a recognized standard source or transfer standard, to which all similar measuring channels in the overall program are referenced, or will be referenced in the future. In other words, this is the residual error between the limiting mean of the measured quantity and the "true" value as established by the standard source or transfer standard used. In these requirements systematic error is stated in terms of error bounds.

### Systematic Error Drift

The variation of the systematic error (defined above) with time for periods exceeding one month for the same radiative flux field, including both shortwave and longwave energy.

### Reproducibility (commonly called Precision)

The random uncertainty of a measurement. In the following requirements precision is stated for 3 sigma limits. The precision values shall be interpreted as measurement random error variation over any one-month interval during the mission for all channels except the solar monitor channel. Included are random errors between measurements within an orbit, from orbit to orbit, and from day-to-day over a one-month period. Any error variation with a time period exceeding one-month shall be considered a systematic error.

For the solar monitor channel precision shall be defined as above for all measurements taken during a solar irradiance determination.

Systematic Error Proportional Component

This is that part of the systematic error (defined above) which is a function of the radiative flux field. The bounds on the proportional component are expressed as a linear function of the magnitudes of shortwave and longwave irradiance or radiance within the sensor FOV.

The standard source may, of course, be different for channels of different spectral responses. The systematic error indicated shall be a requirement not only for initial calibration but shall be maintained throughout the mission. It should be noted that both systematic and precision requirements given in Table A.1 shall be met in the flight environment for at least 2 years mission life in orbit. The notes referenced in Table A.1 define terms and parameters in this table. Brackets {} in Table A.1 and the "Notes" denote design goals.

In addition to the performance requirements given in Table A.1, there is a requirement for monitoring the long-term changes in the monthly mean global and hemispheric shortwave and emission irradiances from the Earth atmosphere system. This requirement places limits on the longterm drift of the systematic (or non-random) errors of the ERBE solar monitor and WFOV instruments.

If the actual systematic error in the WFOV shortwave, WFOV total, and solar monitor channels are $V_i$, $c_i$, and $s_i$, respectively, on the first month of instrument operation and $V_i'$, $c_i'$, $s_i'$ are the corresponding values at any other month in the next 2 years of instrument operation, then requirements are to keep:

$$|V_i - V_i'| < 3.0 \text{ W/m}^2$$

$$|c_i - c_i'| < 1.5 \text{ W/m}^2$$

$$|S_i - S_i'| < 3.0 \text{ W/m}^2$$

for identical radiative fluxes at the spacecraft. A goal shall be to reduce these systematic error drifts to the following design goals:

$$|V_i - V_i'| < 1.0 \text{ W/m}^2$$

$$|c_i - c_i'| < 0.3 \text{ W/m}^2$$

$$|S_i - S_i'| < 1.4 \text{ W/m}^2$$

| CHANNEL DESCRIPTION | RANGE[1] | REQUIREMENTS: PRECISION[5] ($3\sigma$-VALUE) | REQUIREMENTS: SYSTEMATIC ERROR BOUNDS | REQUIREMENTS: SYSTEM ERROR[4] PROPORTIONAL COMPONENT |
|---|---|---|---|---|
| Nonscanner: | $I_T$ ($W/m^2$) | ($W/m^2$) | ($W/m^2$) [2] | ($W/m^2$) [2] |
| WFOV total (AEM) | 80 to 660 | ± 1.5 plus | $\pm [c + d(\lvert I_o - I_T \rvert)]$ | $\pm [d(\lvert I_o - I_T \rvert)]$ |
| (TIROS) | 75 to 620 | | | |
| MFOV total (AEM) | 35 to 400 | ± 0.3% of $I_T$ | | |
| (TIROS) | 17 to 370 | | | |
| | $I_R$ | | | |
| WFOV (AEM) | Zero to 490 | | | |
| Shortwave (TIROS) | Zero to 460 | ± 2.0 plus | $\pm [V + a(I_E - 190)]$ [3] | $\pm [a\lvert(I_E - 190)\rvert]$ [3] |
| MFOV (AEM) | Zero to 295 | | $+ [b(I_R - 100)]$ | $+ b\lvert(I_R - 100)\rvert$ |
| Shortwave (TIROS) | Zero to 275 | ± 0.3% of $I_R$ | | |
| Scanner | ($W/m^2$-sr) | ($W/m^2$ sr) | ($W/m^2$ sr) (6) | |
| | $P_T$ | | | |
| Total | Zero to 500 | ± 0.5 plus ± 0.3% of $P_T$ | ± 2.0 {± 1.5} | |
| | $P_E$ | | | |
| Longwave | Zero to 180 | ± 0.7 plus ± 0.3% of $P_E$ | ± 2.5 {± 1.5} | |
| | $P_R$ | | | |
| Shortwave | Zero to 425 | ± 0.7 plus ± 0.3% of $P_R$ | ± 2.5 {± 2.1} | |
| Solar Monitor | ($W/m^2$) 1290 to 1440 1367 Average | ($W/m^2$) ± 4.2 {±2.8} | ($W/m^2$) ± 7.0 {± 1.4} | |

Brackets { } denote design goals.

See Notes on next page.

Table A.I

NOTES:

(1) Ranges shown are Earth-viewing $I_T$ and $I_R$, except for the solar monitor Note that all channels will view space and the Sun. The ranges of $I_E$ for the nonscanner total and shortwave channels are:

WFOV = AEM ..... 80 to 400 $W/m^2$
TIROS ... 75 to 375 $W/m^2$

MFOV = AEM ..... 35 to 175 $W/m^2$
TIROS ... 17 to 90 $W/m^2$

(2) WFOV

| | c | d | $I_o$ |
|---|---|---|---|
| AEM | 3.4 {1.5} | 0.01 {$3.8 \times 10^{-3}$} | 290 $W/m^2$ |
| TIROS | 3.5 {1.7} | 0.01 {$3.8 \times 10^{-3}$} | 290 $W/m^2$ |

MFOV

| | | | |
|---|---|---|---|
| AEM | 3.1 {2.3} | 0.01 {$3.8 \times 10^{-3}$} | 150 $W/m^2$ |
| TIROS | 3.8 {2.8} | 0.01 {$3.8 \times 10^{-3}$} | 80 $W/m^2$ |

(3)

| | a | b |
|---|---|---|
| $I_E \geq 190$ & $I_R \geq 100$ | 0.01 {0.01} | 0.01 {$6.75 \times 10^{-3}$} |
| $I_E < 190$ & $I_R \geq 100$ | 0.01 {$6.11 \times 10^{-3}$} | 0.01 {$8.92 \times 10^{-3}$} |
| $I_E < 190$ & $I_R < 100$ | 0.01 {$7.5 \times 10^{-3}$} | 0.01 {$5.0 \times 10^{-3}$} |
| $I_E > 190$ & $I_R < 100$ | 0.01 {0.01} | 0.01 {$2.0 \times 10^{-3}$} |
| For WFOV, V = 5.0 $W/m^2$ | {3.0 $W/m^2$} | |
| For MFOV, V = 3.3 $W/m^2$ | {2.0 $W/m^2$} | |

$I_R$ = Earth reflected solar irradiance within the FOV at spacecraft altitude, $W/m^2$
$I_E$ = Earth emitted longwave irradiance within the FOV at spacecraft altitude, W/m
$I_T = I_E + I_R$

$P_R$ = Earth reflected solar radiance within the FOV, $W/m^2$-sr

$P_E$ = Earth emitted radiance within the FOV, $W/m^W$- sr

$P_T = P_R + P_E$

(4) There is a scientific requirement for monitoring the spatial differences (sometimes called the "gradients") of the monthly mean flux densities for both emitted and solar reflected exiting radiation. Errors in the inferred spatial gradients would not result from fixed systematic measurement errors; however, errors in the inferred spatial gradients would be expected to result from systematic measurement errors which are correlated with the irradiances being measured. This requirement limits the acceptable systematic error sensitivities with respect to the irradiances within the FOV of the nonscanner total channel. Denoting by $C_o$ the actual systematic error of either nonscanner total channels at $I_T = I_0$ and the actual systematic error at any $I_T$ (within the appropriate range given in Table A-1) by $C_T$, the Contractor shall demonstrate by analysis and testing that

$$|C_T - C_o| \leq d(|I_o - I_T|)$$

See Notes (2) and (3) for definitions of d, $I_o$, and $I_T$. Denoting the actual systematic error of either nonscanner shortwave channel at $I_E$ = 190 $W/m^2$ and $I_R$ = 100 $W/m^2$ by $V_o$, and the actual systematic error at any $I_E$, $I_R$ combination (within the appropriate ranges given in Table A-1 and Note (2)) by V, the Contractor shall demonstrate by analysis and testing that

$$|V - V_o| \leq a(|I_E - 190|) + b(|I_R - 100|)$$

See Note (3) for definitions of $I_E$, $I_R$, and of a and b for minimum requirements and for design goals.

(5) The precision values given shall be interpreted as random measurement error variation over any one-month interval during the mission. Included are random errors between measurement within an orbit, from orbit to orbit, and from day to day over a one-month period. Any error variations with time periods exceeding one month shall be considered as systematic errors.

(6) The scanner systematic error bounds specified in Table A-1 are for the nominal Earth-viewing radiances:

Total channel - Total radiances = 115 $W/m^2$ - sr
Shortwave channel - SW radiance = 38 $W/m^2$ - sr
Longwave channel - LW radiance = 76 $W/m^2$ - sr

For all Earth-viewing radiances, the scanner systematic error bounds are, for the minimum requirements:

| | |
|---|---|
| Total channel, ± the larger of | 2.0 $W/m^2$ - sr<br>1.7% of $P_T$ |
| SW channel, ± the larger of | 2.5 $W/m^2$ - sr<br>3.5% of $P_R$ |
| LW channel, ± the larger of | 2.5 $W/m^2$ - sr<br>2.0% of $P_E$ |

and, for the design goals:

| | |
|---|---|
| Total channel, ± the larger of | 1.5 $W/m^2$ - sr<br>1.3% of $P_T$ |
| SW channel, + the larger of | 2.1 $W/m^2$ - sr<br>2.0% of $P_R$ |
| LW channel, ± the larger of | 1.5 $W/m^2$ - sr<br>1.0% of $P_E$ |

$I_T$, $I_E$, and $I_R$ are defined in Note (3).